Ecole Polytechnique Fédérale de Lausanne

Laboratoire de physique des hautes énergies

Master thesis

Search for extended gamma ray emission around TeV-class blazars

Author:
David François Droz

Director:
Prof. Dr. Aurelio Bay

Supervisor:
Prof. Dr. Andrii Neronov

June 17, 2016

Abstract

The origins of astrophysical magnetic fields is an open question in physics. Their influence can be indirectly measured in gamma ray astronomy by probing extended emissions around TeV-emitting objects, resulting of particle induced cascades in the intergalactic medium. We investigate the possibility of detecting said extended emission in the Pass 8 data set of the Fermi Large Area Telescope, corresponding to 8 years of measurements between 20 MeV and 300 GeV. By analysing the emissions from nearby pulsars we study the telescope point spread function and establish a reference curve to which we compare the angular photon distribution from BL Lacertae types of blazars. We do not detect any statistically significant extended emission from Markarian 421, Markarian 501 and PKS 1424+240, but from the bounds obtained we were able to exclude extragalactic magnetic fields with a strength between $5 \cdot 10^{-17}$ and $3 \cdot 10^{-15}$ Gauss.

Résumé

L'origine des champs magnétiques cosmiques fait partie des questions toujours ouvertes en physique. Leur influence peut être observée indirectement via l'astronomie en rayons gamma, en inspectant de potentielles émissions étendues autour d'objets émettant dans le TeV. Celles-ci résultent de cascades électromagnétiques induites par un photon à très haute énergie. Le présent document recherche des observations d'émissions étendues dans les données de la *Pass 8* du *Large Area Telescope* à bord de l'observatoire spatial Fermi, qui correspondent à 8 ans de mesures entre 20 MeV et 300 GeV. L'analyse des émissions gamma de pulsars proches permet d'étudier la fonction d'étalement du point du télescope et d'établir une courbe de référence, contre laquelle sont comparées les distributions angulaires de photons venant de blazars de type BL Lacertae. Aucune émission étendue significative n'est détectée autour de Markarian 421, Markarian 501 et PKS 1424+240, mais les bornes obtenues permettent d'exclure des valeurs du champ magnétique extragalactique entre $5 \cdot 10^{-17}$ et $3 \cdot 10^{-15}$ Gauss.

Contents

1 Introduction

The origin of magnetic fields in galaxies and galaxy clusters is still an open question in astrophysics and cosmology. The commonly accepted hypothesis is that they result of the amplification of much weaker fields, whose nature is currently largely unknown. Astrophysical models propose a generation by the motion of plasmas in proto-galaxies while cosmological models suggest that an initial seed field is produced in the early Universe. Recent and current searches look for weak unamplified extragalactic magnetic fields using the tools provided by gamma ray astronomy. However the results are limited to bounds on its magnitude.

The Fermi gamma ray space telescope is a high energy photon observatory currently in operations in Earth orbit. It has been taking measurements since its launch in 2008 and gradually improving our knowledge of high energy phenomena in the Universe. Nearly 8 years worth of data allow for an unprecedented accuracy. Using the Fermi data may allow to tighten the current bounds on cosmic magnetic fields or perhaps detect this elusive field.

The present work proposes to study extended gamma ray emissions resulting from a TeV-photon induced particle cascade in the extragalactic medium. Bounds on the magnetic field can result from the detection, or lack thereof, of a diffuse gamma ray component around TeV-class blazars. This document first introduces gamma ray astronomy, gamma-sources and detecting techniques, as well as presenting the Fermi space observatory, its main instruments and the available data. The chosen analysis method is then described in extensive details, including data selection, considerations on the detector angular resolutions and noise treatments. Finally the main results are exposed and discussed.

1.1 Gamma ray astronomy

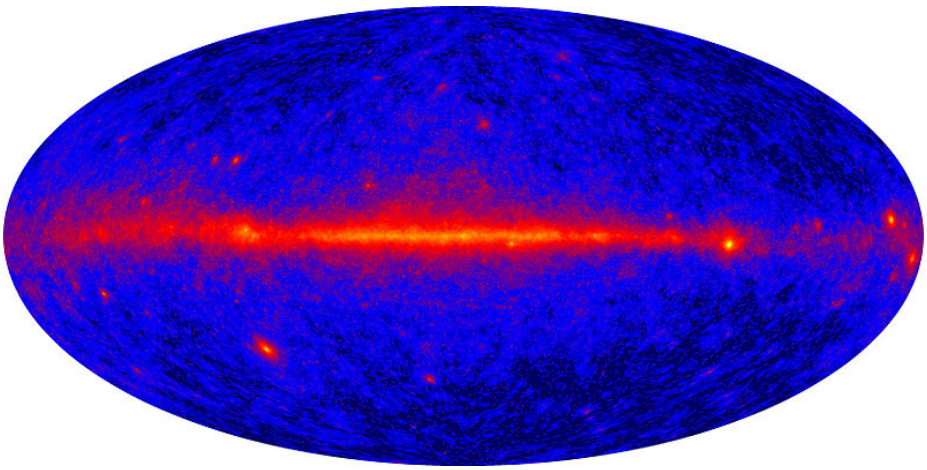

Figure 1.1 – *Full sky in gamma rays as observed by Fermi LAT.*
Image Credit: NASA/DOE/Fermi LAT Collaboration

Gamma rays (often denoted γ rays or simply γ) are extremely low wavelength electromagnetic radiation and consist of very high energy photons. They lie at the high end of the electromagnetic spectrum with energies extending from 100 keV [1] upwards with some recorded events being well above the TeV range.
On Earth they are naturally produced by the radioactive decay of naturally unstable atomic nuclei. A secondary source comes from the interaction of high energy cosmic rays in the atmosphere, or from lightning strikes and other storm-related phenomena in the MeV range.
With the development of modern astrophysics in the 1940s, it was theorised that several processes in the universe should be emitting gamma rays. However this radiation is stopped by the Earth atmosphere and it wasn't until the development of space rockets that we were able to send detectors into orbit. It was noticed that the sky is very bright in gammas, as demonstrated for example on the full sky picture (fig. 1.1) taken by the Fermi space telescope.
We review below the different sources of astrophysical and cosmic gamma rays as well as the current technology to detect and study them.

[1] 10^5 times the energy of visible light, with a wavelength smaller than atoms

1.1.1 Gamma ray astrophysical sources

The closest primary gamma ray source is the Sun. Transient events such as solar flares can produce MeV-range photons along other energetic particles. The Earth atmosphere also produce gammas through interaction with cosmic rays.
Other sources of gamma rays are outside the solar system. There is a diffuse background (Diffuse Gamma Ray Background, DGRB [1]), a nearly isotropic signal covering the whole sky and thought to be mainly of extragalactic origin[17]. Contributors to the DGRB include gammas produced by particle interaction in the intergalactic gas as well as a background of far-away unresolved sources. Annihilation of hypothetical dark matter particles are theorised to produce gamma rays as well [21]. The dominant diffuse background is however the Milky Way galaxy.
High energy gamma rays are also produced by transient events: supernovae, gamma ray bursts (GRB). A supernova is the explosive death of a massive star when it collapses on its core after having burned all its fuel. Such events release electromagnetic radiation over the whole spectrum, including gamma rays and can be brighter than a whole galaxy. They can last from a few days to a couple of months. GRBs are sudden flashes of gamma rays constituting the most energetic electromagnetic event known in the universe. The burst can last from a few milliseconds to several hours. Their origin is still subject to research [51] and might be linked to supernovae [49]. Although bright, both events are very short-lived.
There are finally long duration gamma ray sources such as pulsars and active galactic nuclei that are described below.

Pulsars

Pulsars are a type of fast rotating, electromagnetic radiation emitting neutron star left as remain after a core-collapse supernova.
In broad terms, a star is in an equilibrium state between two forces: gravity, which tends to make massive objects collapse on themselves, and nuclear fusion which produce enough heat and pressure to make the star expand. Both contributions cancel each other during most of its life time. The star will initially burn hydrogen and helium in its core, producing heavier elements. When running out of hydrogen the energy output and therefore the radiative pressure decreases which leads to a contraction of the star and the ignition of the next stage of nuclear fusion.

If the star is massive enough, the nuclear reaction chain will produce and burn heavier elements up to iron. At that point the process stops: the binding energy of nuclei heavier than iron is lower than that of iron and therefore the nuclear fusion isn't energetically possible. The star forms an iron core that contracts until the pressure of the degenerate electron gas inside matter is strong enough to counteract gravity.
Fusion of lighter elements keeps running and producing iron that increase the mass of the core until it reaches the Chandrasekhar limit : $M = 1.4M_{\odot}$, and the core enters gravitational collapse.

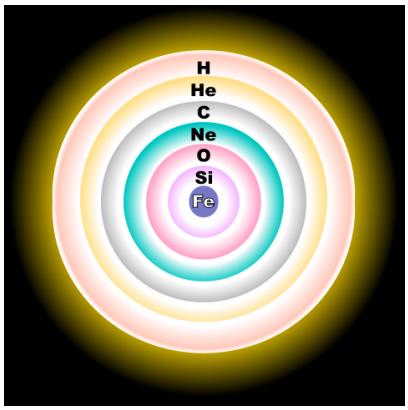

Figure 1.2 – *The onion-like layers of a massive, evolved star just prior to core collapse (Not to scale).*

Image Credit: R.J. Hall, 2007, GNU GPL.

As the core collapses, protons and electrons combine to form neutrons and neutrinos. In a process not yet fully understood, a neutrino burst is produced and transfers enough energy to the star outer layers to release a supernova [50]. The remaining core reaches the density of an atomic nucleus as it becomes a neutron star. Depending on its mass, the neutron pressure can stabilise the core or it can continue collapsing down to a black hole.
The neutron star is a very compact object with a radius of the order of 10km and a mass of the order of 1.5 solar masses. Due to its small size it has a very strong magnetic field and very fast rotation speed. The spin period can be shorter than one second, sometimes down to the millisecond.
Pulsars are a subcategory of young neutron stars. They emit a strong pulsed electromagnetic emission with a period between 1 ms and 10 s as a beam that can be observed when it points toward the Earth, much like a lighthouse. Said beams are visible e.g. in X-rays and gamma rays. Some well known examples include the Crab pulsar (remnant of a supernova observed in 1054 A.D.), Geminga, and the Vela pulsar that due to their vicinity with the Earth are some of the brightest gamma ray sources in the sky at energies below 10 GeV. As such they are prime objects of interest in gamma ray astronomy.

Active galactic nuclei

An *active galactic nucleus* (AGN) is the central part of a galaxy with a much brighter luminosity in comparison to a standard galactic core. Their emission cover most if not all the electromagnetic spectrum, from radio waves to gamma rays up to and beyond the TeV range. They constitute some of the brightest objects in the known universe, reaching luminosities over 10^{45} erg/s, outshining their host galaxy or entire non-active galaxies.

The emission comes from a very compact region having an estimated mass of the order of millions to billions of solar masses. As such the suspected mechanism is the accretion of matter onto a supermassive black hole. Such accretion can produce steady jets of relativistic matter which in turn produce photons over the whole spectrum by synchrotron radiation and inverse-Compton scattering.

Due to their large distance, small size and high luminosity AGN typically have a similar appearance as a star in optical band. A subcategory has thus been historically named *quasar* (quasi-stellar radio source). Other subcategories have been discovered since then: Seyfert galaxies, blazars, radio-loud and radio-quiet quasars, radio galaxies. They differ by their characteristic spectra. Some models suggest that the main difference between these types is our position relative to the jet (if the jet is pointing toward the Earth or at an angle) [11] but observational evidence suggest that the model must be completed [44].

AGN constitute the main sources of gamma rays in the sky. The Fermi's Large Area Telescope second source catalog (2FGL) found 1873 gamma-emitting objects, 57% of which being blazars plus 31% of unknown sources and 6% of pulsars [35].

Point source flux

The gamma ray flux from a point source strongly depends on energy. In some ranges it can follow a *power law*. An example of such power law is given in the Fermi documentation[14]:

$$\frac{\mathrm{d}N_\gamma}{\mathrm{d}E}(E) = A\left(\frac{E}{E_0}\right)^{-\Gamma+2} \tag{1.1}$$

where A, E_0 and Γ are designed in Fermi nomenclature as prefactor, scale and index respectively. The indexes of many gamma sources are listed in catalogs.

The power law is valid up to a certain energy (*cut-off*), where the spectrum drops

sharply. Pulsar spectra have an expected cut-off around the 10 GeV range. AGN can go much higher, up to several hundred GeV or even to several dozens TeV depending on the type of AGN.

1.2 Extended emissions from cascades in the intergalactic medium

Gamma-emitting objects such as pulsars and quasars will appear as point sources due to the important distances and relative compactness. Effects such as gravitational lensing can curve photons in their way to the observer, but as all photons will be curved in the same way the final image will stay point-like.
Other effects can however break this feature and result in a so-called *extended emission*. These are related to particle physics phenomena and processes. An example of such effect is shown on figure 1.3. A high energy ($>$ TeV) photon emitted by an AGN can undergo pair-creation by interaction with the intergalactic background light (photon-photon interaction)[22][23] or with the intergalactic medium. Depending on the presence and magnitude of an intergalactic magnetic field, the resulting e^+e^- pair can be curved and will emit additional photons by inverse Compton scattering and induce electromagnetic cascades. This will in return produce gamma rays of lower energy ($\sim$ GeV) that can travel up to the Earth. The observer will see this secondary photon arrive with a certain angle in comparison to directly observed gamma rays. This angle is expected to be of the order of 1.0° in the Fermi LAT energy range for certain range of intergalactic magnetic fields strength[33]. The actual size and shape depends on the field strength, on the AGN jet orientation and on the spectral characteristics of the source. An isotropic *halo* can be expected if the magnetic field is strong enough[9].
This deviation implies the existence of a magnetic fields. Measurements have already showed the existence of said fields at nearly all scale, from stars to galaxies and even to voids in the large scale structures[15]. Their origins remain however uncertain: magnetic fields dissipate their energy into turbulent and thermal motions of astrophysical plasmas in a time scale shorter than the livetime of the objects carrying them. A regeneration mechanism must therefore exist to explain their existence in the present epoch. A commonly accepted hypothesis is that the magnetic fields are generated by amplification of pre-existing *seed* fields via

dynamo effects. This tiny although non-zero seed field might be generated by a mechanism prior to the formation of large scale structures[16]. The questions remains open as both its strength and origin are uncertain.
One could estimate the magnetic field effect on the properties of extended emission. The typical size of an angular emission due to a cascade appears to be[32]:

$$\Theta_{\text{ext}} = \begin{cases} 0.5^\circ (1+z)^{-2} \left[\frac{\tau}{10}\right]^{-1} \left[\frac{E_\gamma}{0.1\text{TeV}}\right]^{-1} \left[\frac{B}{10^{-14}\text{G}}\right] & \lambda'_B \gg D_e \\ 0.07^\circ (1+z)^{-1/2} \left[\frac{\tau}{10}\right]^{-1} \left[\frac{E_\gamma}{0.1\text{TeV}}\right]^{-3/4} \left[\frac{B}{10^{-14}\text{G}}\right] \left[\frac{\lambda_{B_0}}{1\text{kpc}}\right] & \lambda'_B \ll D_e \end{cases} \tag{1.2}$$

where z is the redshift, τ the optical depth, E_γ the photon energy, B_0 the present epoch magnetic field, λ_{B_0} the corresponding correlation length, D_e the electron cooling distance.
Searches for extended emissions are currently ongoing[45][43] and have been able to derive bounds on the extragalactic magnetic fields. As the Fermi LAT continues to take measurements, the overall accuracy of the analysis increases and we can expect to improve the boundaries or finally to measure the extragalactic magnetic field using the gamma ray data.

1.3 Gamma ray detection techniques

Astrophysical gamma rays are stopped by the atmosphere and do not reach the Earth surface. Moreover due to their high energy it is impossible to use mirrors and other focusing techniques common in optical telescopes. The particle flux (number of particles per unit area and time) is significantly lower than at lower energies, thus requiring high exposure times to produce images and data.
There are two main techniques to detect gamma rays of spatial origin. Direct detection is achieved with pair-conversion telescopes on satellites. At higher energy the radiation is detected indirectly by particle reactions in the upper atmosphere using Cherenkov telescopes. We list and describe both techniques below for the sake of completeness. In the scope of this work we will exclusively use data from the Fermi LAT, a pair-conversion telescope.

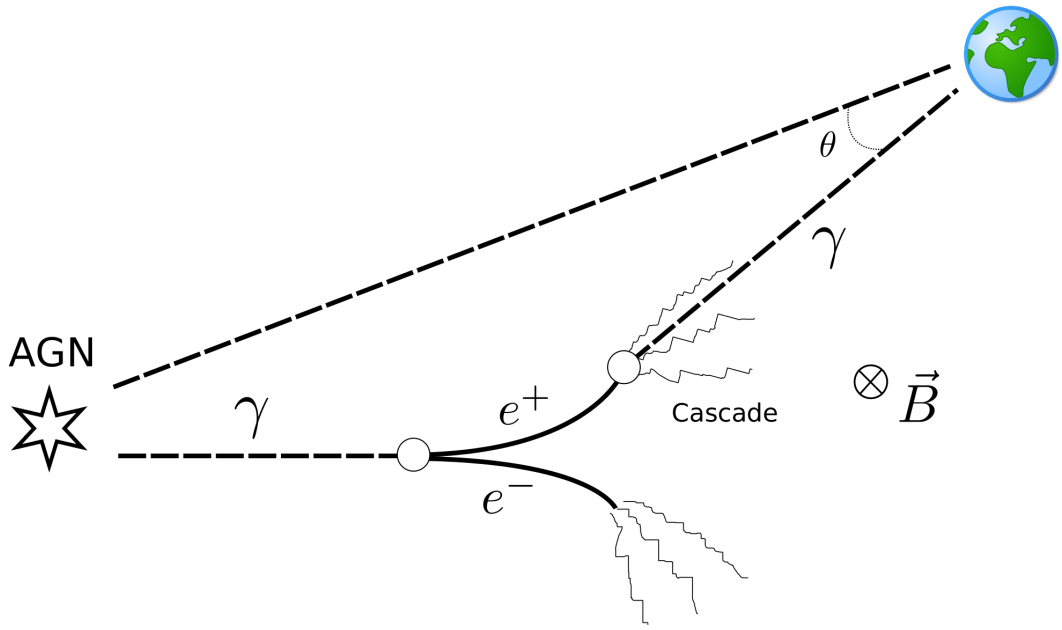

Figure 1.3 – *Principle of an extended emission: a gamma (γ) ray produced by an AGN interacts in the intergalactic medium. The e^+e^- pair is curved by a magnetic field $\vec{B}$ and undergoes further interactions (cascade). A lower-energy γ arrives on Earth with an angle θ with respects to the direct line of sight.*

Own work, with elements from Wikimedia Commons , GNU GPL.

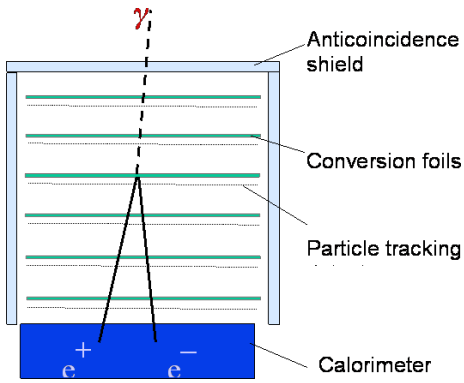

Figure 1.4 – *Concept of a pair conversion telescope.*

Image Credit: NASA/DOE/Fermi LAT Collaboration

1.3.1 Pair-conversion telescopes

The most direct way to detect gamma rays is to set up a particle detector outside of the Earth atmosphere, for example in Earth orbit or beyond. These instruments are called *pair-conversion telescopes* due to their principle of operations.

The concept is reported in figure 1.4. An incoming high energy photon enters the telescope and goes through thin layers of dense metal until producing an electron-positron pair: $\gamma \rightarrow e^+e^-$. The two leptons then travel through a particle tracker, usually layers of semiconducting material that are ionised when a charged particle flies through. Picking the position of the successive signals gives the trajectory of the two $e^{+/-}$. Finally these two particles reach an electromagnetic calorimeter where they deposit all their energy. By conservation laws, the incident photon can be fully reconstructed with an accuracy limited by the performances of the detector: size and density of the tracking pixels, size of the calorimeter, and so on. Background rejection is performed with an anti-coincidence detector: a neutral photon will fly through without interacting while a charged particle will leave a signal, usually ionising light.

While pair-conversion telescopes are the most straightforward way of detecting astrophysical gamma rays, being space-based impose strong limitations on the technology. Specifically, their mass is limited by the rocket technology (payload and cost) and by the difficulties of operating in the space environment: low pressure, large temperature range, radiation damage and the lack of any possible mainte-

nance. Nevertheless there have been numerous gamma ray space observatories, including NASA's *Fermi Gamma-Ray Telescope* which registered the data used in the present work (section 1.4)[2].

1.3.2 Cherenkov telescopes

At energies above 100 GeV the cosmic rays flux drops sharply, with around 1 TeV-class event per minute and per square meter over the whole sky and 1 PeV-class event per year and per square meter [40]. At such energies space-based detectors are inefficient due to their limited collection area (Fermi telescope: 0.8 m^2).
Ground-based telescopes use the Earth atmosphere as a detection medium. When a very high energy gamma ray enters the upper atmosphere it undergoes a pair production process. The electron and positron will immediately dissipate their energy through Bremsstrahlung and thus produce additional gamma rays that themselves create a new electron pair. The whole process leads to a cascade of particles called an *extensive air shower*. Particles in the shower are ultra-relativistic and will release UV light through Cherenkov radiation. This UV flash can be detected from the ground and used to reconstruct the initial photon.
Currently operating Cherenkov telescopes include HESS[25], MAGIC[28], VERITAS[47]. They typically operate above ∼30 GeV. Since the signal we're looking for is approximately in the 1 - 10 GeV range, we will not use data from Cherenkov telescopes.

1.4 The Fermi space telescope

The *Fermi Gamma-ray Space Telescope* (hereafter *Fermi*) is an Earth-orbiting, high energy photons detector and gamma-ray bursts monitor[37]. The mission, lead by NASA with contributions from France, Germany, Italy, Sweden and Japan, was launched in June 2008 aboard a Delta II heavy launch vehicle. Originally known as GLAST, it was renamed in honour of physicist Enrico Fermi.
Fermi's mission is to study the gamma ray emissions in the universe. This includes the observation of AGN, neutron stars, supernovae remnants, gamma bursts, the background radiation, solar flares, emissions from the Milky Way galaxy, as well as potential signal from dark matter and tests of fundamental physics[31]. The mission has already scored a number of discoveries and important observations[2][3][41].

[2]Other current observatories include INTEGRAL[48], AGILE[42], Swift[19]

The spacecraft was injected into low earth orbit at an altitude of 550 km and 25.6° inclination. The mission is planned to last for 5 to 10 years, of which 8 years have already passed. It orbits the Earth in 95 minutes, pointing its main instruments away from the Earth and follows a "rocking" motion to increase coverage of the sky. The telescope covers the whole sky in two orbits, or three hours.
Fermi embarks two instruments. The main detector is the *Large Area Telescope* (LAT) which is discussed in details in section 1.4.1 below. The second instrument is the *Gamma Ray Burst Monitor* (GRBM)[29]. Its purpose is to detect and study transient events such as solar flares and most importantly gamma ray bursts, and to transmit the information to the spacecraft such as to orient the main payload in the direction of the burst. It is composed of 12 sodium iodide scintillation detectors and 2 bismuth germanate scintillators covering together a range between 8 keV (hard X-ray) to 30 MeV (lower limit of the LAT). The modules are distributed around the spacecraft to cover the whole sky.

1.4.1 Large Area Telescope

The main instrument of the Fermi is the *Large Area Telescope* (*LAT*)[13]. It is a wide field of view, gamma ray pair-conversion telescope (fig. 1.4). It is sensitive to γ from 20 MeV to 300 GeV and above.
The LAT measures the individual tracks of the e^+ and e^- resulting of a pair-production process from an incident gamma ray, and measures the energy of the subsequent electromagnetic shower in a calorimeter. It was built to have a high field of view while rejecting cosmic rays. The instrument consists of a 4×4 array of 16 modules each with a tracker and a calorimeter. All modules operate independently for redundancy purposes. The tracker array is covered by an anticoincidence detector for background rejection.
The tracker[12] consists of 18 x, y tracking planes, each having two thin layers of silicon strip detectors in perpendicular alignment for bi-dimensional measurement. The first 16 layers are interleaved with thin foils of tungsten (high atomic number). An incident photon undergoes a pair-production process in one of the tungsten layers: the produced e^+e^- fly through the silicon strip detectors where their trajectory is measured and leads directly to the direction of the initial photon. The characteristic signal of a pair production also allows background rejection.

The flight direction of the e^+e^- pair is random. The probability distribution is known as the point spread function (PSF, section 2.3). A high PSF means a low angular resolution. The lepton pair can undergo scattering processes in either the tungsten or silicon layers, thus broadening the PSF at low energy. At high energy where multiple scattering is negligible the angular resolution is dictated by the pixel size in strip detectors.
Thin layers can reduce the effect of multiple scattering, but decrease the amount of converter material and therefore lower the effective area. As a balance solution the LAT tracker is separated in two parts, known as *front* and *back*. The first 12 layers (front) have a thickness of 0.03 radiation lengths, and the converters in the back are 6 times thicker to maximise the effective area at the cost of a factor of two on the PSF width at low energies.
The calorimeter serves two purposes[27]: first, it measures the total energy deposited by the particle shower resulting of the e^+e^- pair thus reconstructing the energy of the incident photon. Second, it images the shower development profile to provide background rejection and estimate the energy leakage. Each calorimeter module consists of 8 layers of 96 CsI(Ti) crystals optically isolated from each other, with a total vertical depth of 8.6 radiation lengths. Each layer is perpendicular to its neighbours to get two dimensional measurement of the shower. The crystals are read out by PIN photodiodes.
Fermi LAT energy range is limited by the calorimeter size. Photons above 300 GeVare energetic enough for the electromagnetic shower to not be fully contained in the calorimeter, therefore resulting in a loss of energy resolution.
Charged-particles background rejection is assured by an anticoincidence detector constituted of plastic scintillator tiles distributed around the tracker area. The scintillation light produced by a charged particle is collected both by wavelength shifting fibers and photo-multiplier tubes for redundancy. It achieves an efficiency of 0.9997. The detector is also shielded against micro meteorites.
A full technical description of Fermi/LAT was published by Atwood et al., 2009[13]. We report in table 1.1 a brief summary of its performances and in figure 1.5 the effective area, angular/energy resolution and acceptance dependencies on energy.

Energy range	20 MeV to >300 GeV
Energy resolution	15% at energies >100 MeV
Angular resolution	3.5° (100 MeV), > 0.15° (> 10 GeV)
Effective area	8000 cm^2 (1 GeV, normal incidence)
Field of view	2.4 sr
Deadtime per event	100 μs
Time accuracy	10 μs
Source location determination	0.5 arcmin

Table 1.1 – *Summary of official LAT pre-launch specifications and performances.*

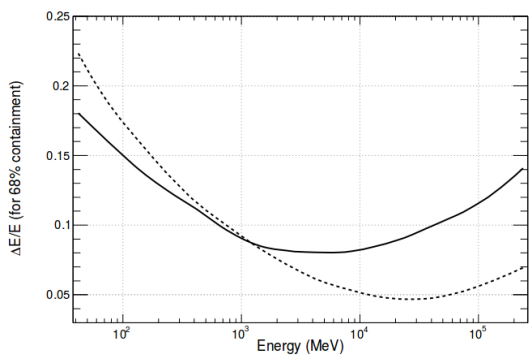

(a) *Energy resolution for normal incidence (solid curve) and at 60° off-axis (dashed curve).*

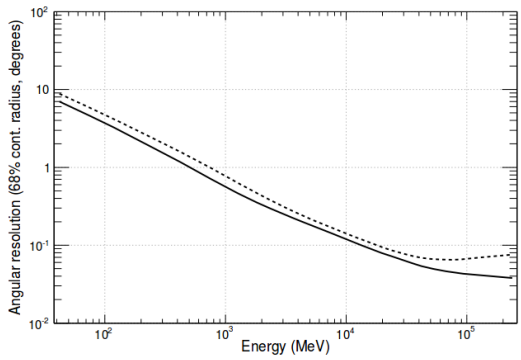

(b) *Angular resolution for normal incidence (solid curve) and at 60° off-axis (dashed curve).*

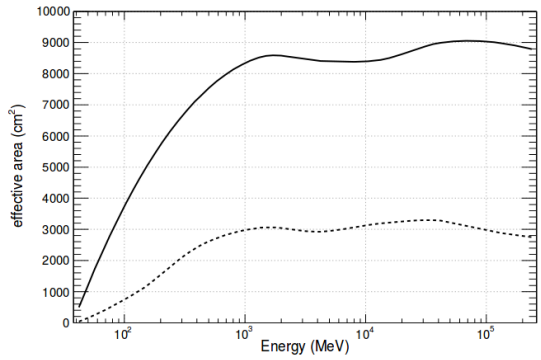

(c) *Effective area for normal incidence (solid curve) and at 60° off-axis (dashed curve).*

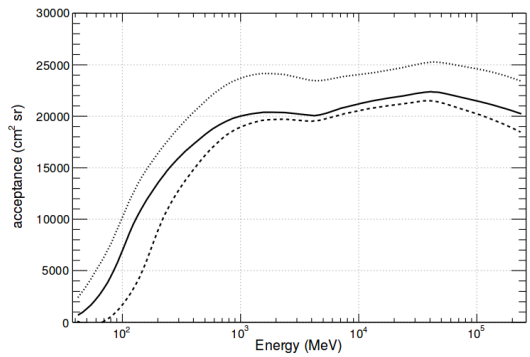

(d) *Acceptance for Diffuse (dashed curve), Source (solid) and Transient (dotted) analysis classes.*

Figure 1.5 – *Fermi LAT performances versus energy.*

Image Credit: Fermi/LAT collaboration, W.B. Atwood et al., 2009. Creative Commons.

1.4.2 Data and software

Fermi LAT data is available publicly through the Science Support Center[30]. It consists of a list of recorded photons, each having associated energy, coordinates, angle of incidence, etc. Each event has a *type* of either `front` or `back` depending on the section of the tracker-converter that triggered the pair conversion. Photons also have a *class* depending on the reconstruction algorithm: `transient`, `source` and `clean` from the loosest to the strongest background rejection. The `source` is the recommended analysis class.

The data is available in `.fits` format. It can be explored using *SAOImage ds9*, *NASA's HEASARC* package, or using astronomy libraries within *Python*. Additionally the Fermi team provides an extensive list of analysis tools for the LAT data, ranging in complexity from simple cuts to model fitting. A full documentation is also provided on the web[14].

A spacecraft file is also provided alongside the data that contains all the information on the Fermi position and orientation over time, which is needed to compute exposure and select the data taken when a source of interest was not occulted by either the Earth or the Sun.

The recommended method is the so-called *likelihood analysis*: the data is selected in a wide circle around a source of interest. Each emission within that radius is then associated to a model, and the flux is computed by performing a maximum likelihood fit of the model on the data. The process must then be iterated to reach a good enough fit. The Fermi tools also support aperture photometry but do not recommend it due to the large angular resolution of the LAT.

The LAT has currently registered 7 years and 10 months of data. The public servers are currently releasing the *pass 8* (P8R2) data set.

2 Search for extended emission

The main goal is to find or to put constraints on extended gamma ray emissions around astrophysical sources. We study photon distribution as a function of distance around specific sources, and compare this evolution to a reference point spread function, in energies between several hundred MeV and a few dozen GeV. We discuss in section 2.2 below the analysis of cumulative distribution curves, in 2.3 the method to obtain an experimental point spread function, and in 2.4 the selection process on gamma ray sources. Noise and noise removal is discussed further below in section 3.

2.1 Data selection

We use the data from the Fermi LAT *Pass 8* with 7 years and 10 months worth of measurements, from August 2008 to May 2016. Sources, source type and coordinate are extracted from Fermi LAT 4-years point source catalog *3FGL*. The event class used is the P8 `source` class as recommended by the official LAT analysis documentation[14]. The data include both `front`-type (event reconstructed in the front part of the tracker) and `back`-type events to maximise statistics. To avoid gamma-ray pollution we apply a cut on the zenith angle of 90°.

2.2 Photon angular distribution

The main method recommended by Fermi LAT is a *likelihood analysis*. While effective to compute spectra it is strongly dependent on an input model for each source in the sky. Modelling an extended emission would require strong assumptions on the energy and shape of the signal. Instead we choose to opt for a model-independent method and use *aperture photometry*.
The shape of an extended emission is a priori unknown. It can be isotropic and therefore have the effect of broadening the signal from a given source. It can also be directed in one particular direction depending on the presence and strength of a magnetic field. We therefore decide to look for the angular photon distribution to suppress any directional bias, following the method illustrated in figure 2.1.

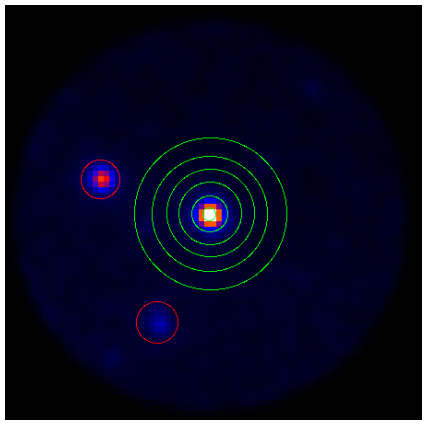

Figure 2.1 – *Illustration of integration method in a LAT picture of blazar* PKS 1424+240 *(7° fov., 500 MeV - 50 GeV, linear colour scale). Photons are counted inside each green circle with a linearly growing radius (angular distance binning). Red circles show polluting γ sources (sec. 3.2).*

We take consecutive circles around the source of interest with a linearly increasing radius and integrate the flux over their surface. Since the number of events is finite, this is equivalent to simply counting the number of photons inside each circle. The result is a cumulative plot as each circle contains the previous one. For a point source and assuming no noise at all, the expected result is a curve similar to figure 2.2 to the right.

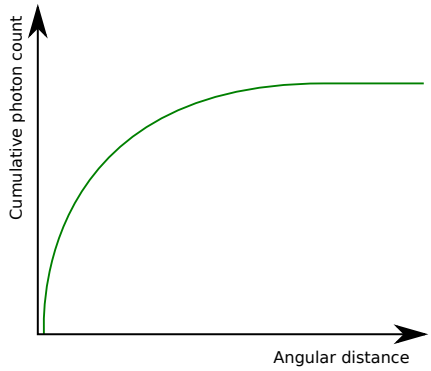

Figure 2.2 – *Cumulative angular photon count for a point source*

An extended emission would have as effect to broaden this distribution: the curve would get flat further away from the source, or show a bump at a certain distance. This effect must then be inspected to see if there are known gamma ray objects in the vicinity, emulating the signal (see section 3 on noise).
To be able to see these effects the distribution must be compared to a reference one, namely the expected distribution of a perfect point-source. It is given by the point spread function that is discussed below.

2.3 Point spread function

Any imaging system such as a camera, telescope and so on, has limitations on its imaging resolution. The Point Spread Function (PSF) characterise the response of that system to an observed point source and how it will reconstruct the image. The PSF is the spatial component of the Fermi LAT instrument response function, with other components being the effective area (efficiency) and the energy dispersion. It is equivalent to the probability distribution function $p(\delta v, E, \hat{v})$ for δv the offset between the true ($\hat{v}$) and reconstructed direction of a detected gamma ray.

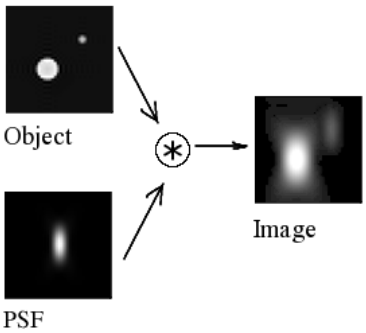

Figure 2.3 – *Image formation in an optical system. The reconstructed image is the convolution of the photon flux with the PSF.*

Image Credit: 'Default007', Wikimedia user, 2006, GNU GPL.

The LAT spatial resolution depends on mainly two factors: at energies below 1-10 GeV, the electron-positron pair created by an incident photon can scatter in the various layers of the instrument. Due to the randomness of multiple scattering, this effects introduces an uncertainty on the direction of the initial event. At higher energies, the spatial resolution is dominated by the accuracy of the silicon tracker, which strongly differs for `front` and `back` events. The PSF is then further affected by the reconstruction algorithms, the event selection and the background rejection processes.

The LAT PSF depends on the energy and inclination of an incident photon, as well as the event type (front and back). The analytical form was derived from XMM and follows the so-called *King function*[14]:

$$K(x, \sigma, \gamma) = \frac{1}{2\pi\sigma^2}\left(1 - \frac{1}{\gamma}\right) \cdot \left[1 + \frac{x^2}{2\gamma\sigma^2}\right] \tag{2.1}$$

where σ is the characteristic size of the angular distribution and γ determines the weights of the distribution tails. This function tends to a normal distribution in the limit $\gamma \to \infty$[7][26]. The Fermi LAT team reports that a single King function does not fully reproduce the observed distribution of reconstructed gamma rays

and introduce a distribution with two King functions:

$$P(x, E) = f_{\text{core}} K\left(x, \sigma_{\text{core}}(E), \gamma_{\text{core}}(E)\right) + (1 - f_{\text{core}}) K\left(x, \sigma_{\text{tail}}(E), \gamma_{\text{tail}}(E)\right) \quad (2.2)$$

where the *core* component characterises the distribution for small angular separations, and the *tail* component for large ones. $P(x, E)$ is then fit over distributions obtained by Monte Carlo simulated data. The parameters are finally released alongside the data and the Fermi science tools. This allowed pre-flight estimates of the PSF, the effective area and the containment radii (fig. 1.5).
After launch and actual data taking it was found that the PSF width had been underestimated at energies above 3 GeV. The PSF had to be experimentally measured from a catalog of point sources[7] and the new parameters are part of the *Pass 8* data release.
The data release and the official PSF are adapted to the likelihood method that we mentioned earlier. Our analysis rely on aperture photometry and we therefore want to build our own "experimental" PSF. Indeed we want to compare quantities obtained by the same analysis method.
The first step to build the PSF is to select suitable sources. These must be point-like, clean of nearby gamma-emitting objects and bright enough to obtain good statistics. The selection process is described further below in section 2.4.1. For each object, the photon distribution is computed as described previously. All the different distributions are stacked together to smooth down unusual features that went through the selection or the noise removal (sec. 3) processes. Finally, the stacked curve is normalised to have a value of 1.0 far away from the center.
The obtained PSF will look like figure 2.2. It is the standard expected distribution for a point source, and any object featuring extended emission will therefore deviate from it. Figure 2.4 shows an example of a distribution from an extended source.

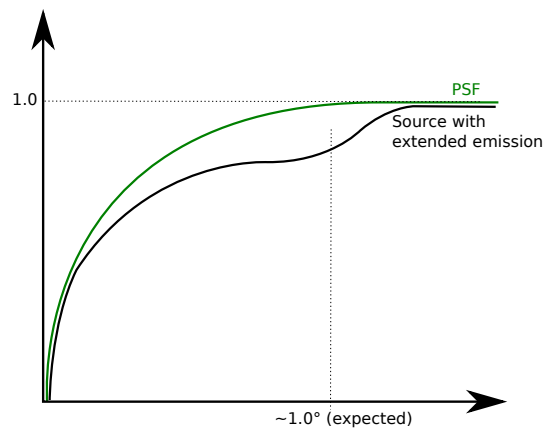

Figure 2.4 – *Schematic view of the kind of signal expected from extended emission.*

2.4 Source selection criteria

We select two different kind of gamma ray sources: "references" used to build the experimental PSF, and "candidates" to look for extended emission. The objects are selected from Fermi LAT 3FGL.
The sources must be point-like, thus excluding nebulae, the galactic plane and other extended objects. Their immediate vicinity as projected on the sky must be clean enough of other gamma-emitting objects (see section 3) and bright enough to study them.

2.4.1 Experimental PSF

Establishing the PSF requires point sources as bright as possible to maximise photon statistics. As we expect potential extended emission in a range between few hundreds MeV and $\sim$ 100 GeV, we want objects that emit in this domain without going to several TeV. Extended emissions are indeed expected to result from photons above the TeV range.
Pulsars meet these requirements. Smaller than a planet they can be considered as point sources. Since our integration time is far greater than their orbital period their oscillatory nature is irrelevant and they can be treated as continuous sources. Some pulsars are among the brightest gamma ray objects in the sky. Their typical spectral cut-off lies around 10 GeV.

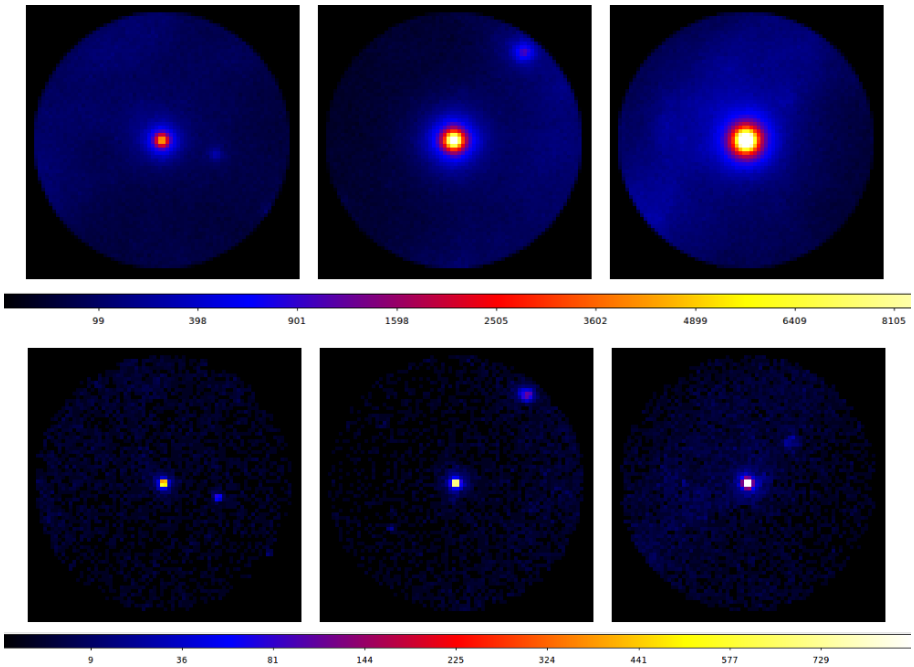

Figure 2.5 – *Fermi LAT 7° field of view around pulsars Crab, Geminga and Vela (from left to right), in the 1 - 1.9 GeV (top) and 7 - 13.5 GeV (bottom) energy ranges. Colour bar shows the number of photons per pixel.*

The first three reference sources are the *Vela pulsar*, *Geminga* and the *Crab pulsar* (fig. 2.5). Vela is the single brightest persistent object in Fermi LAT energy range and is therefore the main component of the PSF. Around 1 GeV these three objects are bright enough to build a full accurate PSF.

At energies slightly below or beyond 10 GeV the pulsar flux drops sharply and we need additional sources to get appropriate statistics. The first idea is to add more pulsars based on the 3FGL catalog. A complication is that pulsars are remains of dead massive stars and are thus found in star-rich areas such as the galactic plane and galactic center. The Milky Way galaxy is a strong source of gamma rays and would therefore pollute the signal.

Based on the 3FGL catalog, we first select the 40 brightest pulsars in the sky. We then exclude the sources lying in the galactic plane or near the core and are left with 11 objects. Their emissions are then analysed by eye using picture visualisation software to remove pulsars having diffuse emission nearby. A final selection is applied by comparing their cumulative photon count to Vela's and Geminga's to

look for any significant deviation. At the end of this process the only remaining pulsar is *CTA 1*. Due to pulsars spectra characteristic drop at 10 GeV, having only pulsars limits the statistics at higher energy.
The main other class of persistent point sources in the gamma ray sky are quasars. However some quasars can emit gamma rays with energies well beyond the TeV range and as discussed further below are therefore prime candidates for extended emissions. We can nevertheless opt for *flat spectrum radio quasars* (FSRQ) without any recorded TeV event. The selection process is made easier by both the 3FGL and TeVcat catalogs[46].
The selection is restricted to the 15 brightest FSRQ in the 10 GeV domain. 5 quasars were flagged by TeVcat as having TeV emissions. The 10 remaining objects were finally inspected by eye to remove unwanted contributions and compared in the 1-10 GeV domain to Vela and Geminga. This leads to two FSRQ objects in complement of the four pulsars. All sources are listed in table 2.1 below.
This selections gives a reference curve from 300 MeV (LAT lower bound) up to 50 GeV where the photon flux is too low for any significant measurement.

	RA [degrees]	**Dec** [degrees]
Vela pulsar	128.836	-45.1764
Geminga	98.4788	17.7732
Crab pulsar	83.6372	22.0241
CTA 1	1.7656	73.0499
3C 454.3	343.5018	16.1459
PKS B1424-418	216.9914	-42.1106

Table 2.1 – *List of objects used to build the experimental PSF.*

2.4.2 Candidates

Candidates for extended emission are TeV-class AGN that are typically detected both by ground-based Cherenkov telescopes and by Fermi LAT. AGN emitting in the TeV range are known as *BL Lacertae* objects, a subcategory of blazars[20].
The first candidate is *Markarian 421*. As one of the closest blazars to Earth, it is one of the brightest quasars in the sky. It emits TeV photons in strong bursts[18]. Due to its high brightness and lack of nearby polluting source it is an easy study

case. On the other hand its low cut-off might imply low energy extended emission. Current searches have only obtained upper bounds[10].
Other candidates are listed in table 2.2 below with sample pictures in figure 2.6.

	RA [degrees]	**Dec** [degrees]	**Redshift z**
Markarian 421	166.114	38.2088	0.031
Markarian 501	253.468	39.7602	0.034
PKS 1424+240	216.752	23.8	0.88 ± 0.28
1ES 0229+200	38.2026	20.2882	0.14

Table 2.2 – *BL Lac objects candidates for extended emission.[46]*

A notable candidate is the blazar *1ES 0229+200*. Originally detected by HESS, it provides tight constraints on the extragalactic magnetic field and background light[8][45]. However as visible in figure 2.6d it is a very weak source. It is in fact so faint that it wasn't detected by Fermi LAT after 2 years of exposure (2 years catalog 2FGL).

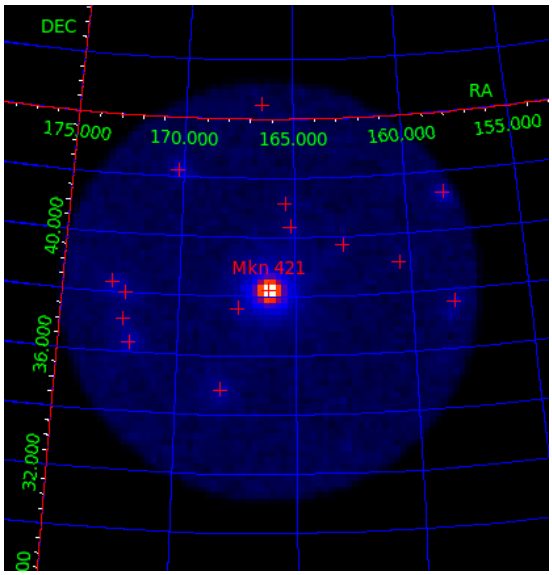

(a) Markarian 421 (max:1120)

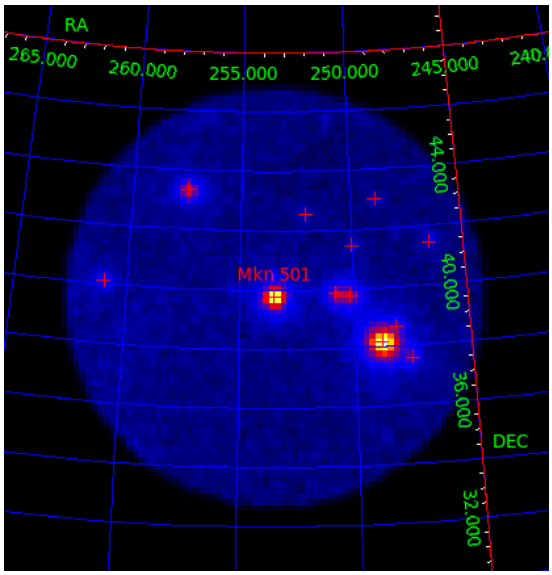

(b) Markarian 501 (max:547)

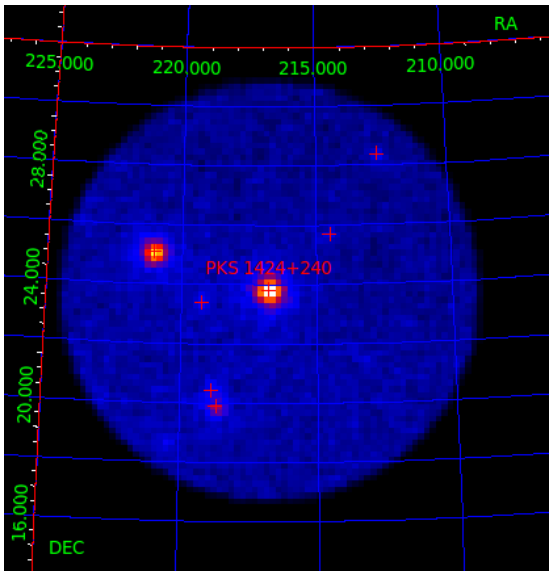

(c) PKS 1424+240 (max:366)

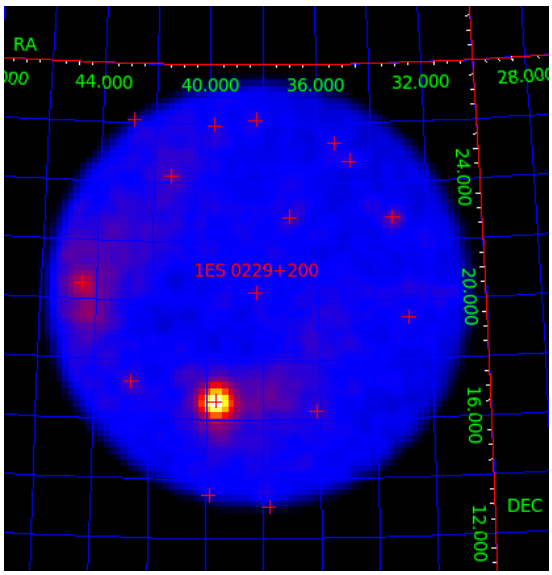

(d) 1ES 0229+200 (max:227)

Figure 2.6 – *Fermi LAT colour map of four BL Lac objects, 600 MeV - 50 GeV, 7° field of view, 8 years of data. Red crosses show 3FGL identified sources. "Square-root" colour scale. Number between parentheses in subcaption show the number of photons corresponding to white colour.*

3 Noise description and treatment

As revealed by the numerous gamma ray telescopes, in particular by Fermi LAT (fig. 1.1), the sky is quite bright in gamma rays. We can therefore expect significant noise and polluting signals when establishing the experimental PSF and when studying a source of interest. We discuss below the different sources of astrophysical noise and present our methods to remove them.

3.1 Diffuse component - galactic foreground, cosmic background

The main pollution source is the Milky Way galaxy in which we reside. The galactic plane appears very clearly in fig. 1.1. Due to its size and brightness, removing its contribution is no easy task. While techniques exist[39], in the scope of this work we decide to only select sources that are distant enough to the galactic plane and galactic center.

An important noise comes from the so-called Diffuse Gamma Ray Background (DGRB). It is a nearly isotropic signal covering the whole sky and thought to be mainly of extragalactic origin: gamma sources with a flux lower than Fermi LAT are not resolved individually but rather form a diffuse glow. Contributions to the DGRB include unresolved blazars, misaligned AGN, star-forming galaxies, millisecond pulsars, distant supernovae, etc. A more exotic contribution would be the hypothetical dark matter particle annihilation or other kind of signals predicted by Beyond-the-Standard-Model theories.

The DGRB is not perfectly isotropic and the diffuse galactic foreground is clearly not. Since we select objects far from bright galactic contributions, and the angular scales considered are not very large, we can work under the isotropic approximation. If $\rho_{\mathrm{D}}(\alpha, \delta)$ is the DGRB flux projected on the sky per unit of solid angle:

$$\rho_{\mathrm{D}}(\alpha, \delta) = \rho_{\mathrm{D}} = \text{constant}$$

The flux over an arbitrary circle S on the sky with an angular radius θ is then:

$$\Phi_{\mathrm{D}} = \iint_{S_\theta} \rho_{\mathrm{D}}(\alpha, \delta) \mathrm{d}\Omega = \rho_{\mathrm{D}} \iint_{S_\theta} \mathrm{d}\Omega \ \propto \ \theta^2$$

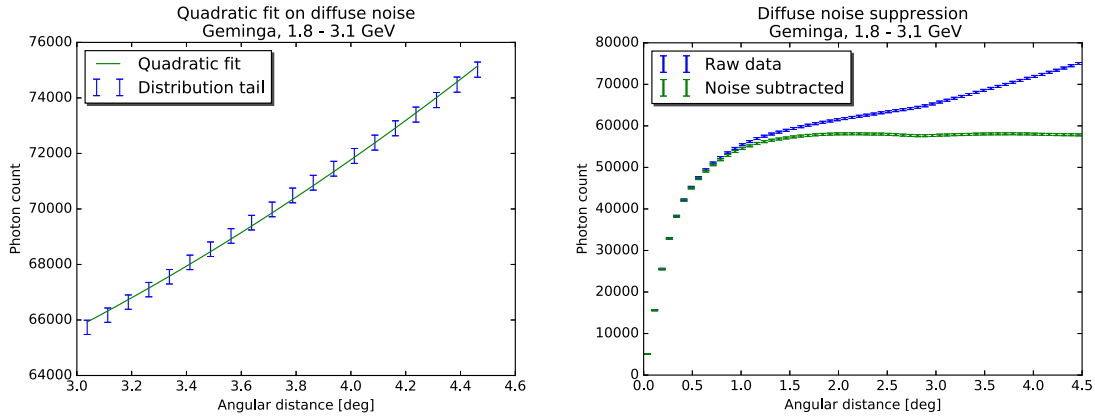

Figure 3.1 – ***Left:*** *Example of a second-order polynomial fit on the tail of the photon distribution.* ***Right:*** *Result of subtracting the fitted function to the whole distribution. The DGRB contribution is removed.*

In other words, a cumulative angular distribution (section 2.2) of the DGRB can be treated as a quadratic function. To characterise that noise in the vicinity of a source of interest, the photon distribution is considered from twice the 95% C.R. to an angular radius big enough to have acceptable statistics and small enough to avoid other sources. That tail is then fit with a second order polynomial of the form $f(x) = ax^2 + b$. The fitted curve is then subtracted to the source photon count in order to remove the DGRB contribution from the analysis (fig. 3.1).

3.2 Secondary point sources

Pulsars, AGN and other gamma-sources located around the source of interest on the sky can have a significant influence on the analysis. A cumulative photon count including such pollution would show sudden increases at some distance away from the source as schematically shown in figure 3.2. The signal depends on the distance and number of sources as well as on the PSF. Depending on energy, polluting signals can either overlap each other or overlap with the main object PSF.
Removing unwanted point sources seems easy at first glance: simply don't take into account photons coming from that source. However proceeding this way also cuts the overlapping diffuse background and can therefore skew the background treatment.

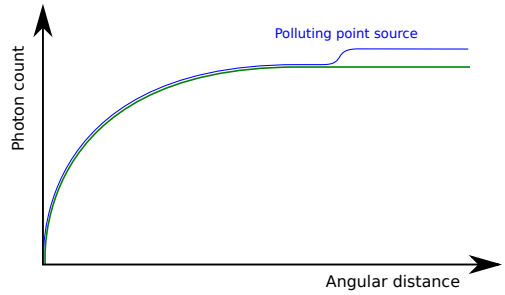

Figure 3.2 – *Influence of a secondary gamma ray point source on the cumulative photon count. Green curve shows the standard count. Blue curve shows a count with such pollution.*

The first step is to identify potentially polluting point-like sources around the studied objects. Reviewing the images (2D binned count maps) by eye can immediately reveal the most important one (see for example fig. 2.1) down to sources having less than 10% of the main object brightness. Fainter sources can be identified by using the 3FGL catalog.
Each polluting source is then associated to a circle on the sky, with an angular radius equal to the 95% containment radius of the PSF. When computing the cumulative photon count for the object of interest, events that originate from within that circle are ignored. Thus successfully removing the noise.
However this treatment also removes background events that were within that circle. We discussed previously that the diffuse background is removed by performing a polynomial fit. However this fit will be skewed as some photons have already been removed. We propose to introduce a Monte-Carlo simulated correction factor to restore the cut background.
The correction factor is estimated using a M.C. simulated background. We first generate a random, uniformly distributed list of events around the object of interest, without having any photon from the source or any physical object.
Given α_S,δ_S the respectively right ascension, declination of a source, we generate couples of coordinates (α, δ) along the following distribution:

$$\alpha = \alpha_S + ((2a-1)\theta) / \cos(\delta_S) \qquad a \in [0,1] \tag{3.1}$$

$$\delta = \delta_S + (2b-1)\theta \qquad b \in [0,1] \tag{3.2}$$

where a,b, are randomly generated and θ is the angular size (in degrees) of the field of view. $\cos(\delta_S)$ appears due to the spherical geometry. This distribution generate a square of dimensions $\sim 2\theta \times 2\theta$ instead of a circle of radius θ. We then select all points such that the angular distance ξ is lesser than θ:

$$\xi \equiv \sqrt{\left((\alpha - \alpha_S)\cos(\delta)\right)^2 + (\delta - \delta_S)^2} \;\leq\; \theta \tag{3.3}$$

The process is then iterated until having 500'000 events within that circle.
A non-cumulative photon distribution is then computed twice from the simulated data: once on the whole circle with no additional constraint, and once with cutting events within circles around polluting sources as explained previously. We then define the correction factor η :

$$\eta(\xi) \equiv \frac{\text{Simulated data, cut } (\xi)}{\text{Simulated data } (\xi)} \tag{3.4}$$

This correction factor is finally applied to the real distribution to restore the lost background while still having cut the contribution from polluting sources.

$$\text{Corrected distribution } (\xi) = \frac{\text{Distribution } (\xi)}{\eta\ (\xi)} \tag{3.5}$$

3.3 Planet Earth

Our own planet emits gamma rays toward space. Production processes include cosmic rays interaction in the upper atmosphere, storms, and mostly from the Earth limb [24]. The LAT data include for each event a *zenith angle*, which is the angle between the photon provenance and the local vertical of the spacecraft. In the data selection process we simply cut all events having a zenith angle greater than 90° as recommended by the Fermi LAT team.

3.4 Other extended objects

Nebulae, supernova remnants and clouds of interstellar gas can produce gamma rays by interaction with cosmic rays. Some of these objects can be close enough to not be point-like sources. Their emission and subsequent pollution on nearby objects is strongly dependent on their shape. As this analysis would be time-

consuming we decide to avoid sources having a bright diffuse object in the immediate vicinity. We discuss below a potential analysis to treat extended objects.

3.5 Statistical noise

Fermi LAT data are lastly subject to instrument and statistical noise. In the case of integer photon count as performed in our work, we model it as shot noise with Poisson statistics. In such a regime and for the large numbers we consider in our analysis, the measurement uncertainty δN is given by:

$$\delta N = \frac{N}{\sqrt{N}} = \sqrt{N} \tag{3.6}$$

where N is the number of events. The larger the number of events, the better the signal-to-noise ratio and the more accurate the results are. Hence the importance of maximising the photon count.

4 Analysis summary

We present here a summary of the analysis method used. `gtselect`, `gtbin` and `gtexposure` are part of the science tools provided by the Fermi team.

Step 1 - Build PSF

1. Source selection
   (a) Browse 3FGL catalog for bright pulsars away from the Milky Way and for FSRQ galaxies
   (b) Inspect 7-8° f.o.v. (count map, `ds9`) around the source to look for pollution
2. Choose an appropriate energy range with logarithmically-spaced bins
3. Build the angular photon distribution for each source (`python`)
   (a) Cut with `gtselect`, 5° f.o.v., 90° azimuthal angle.
   (b) Make a histogram of the photon angular distribution (number of photons versus distance to source)
   (c) Cut away from the histogram the areas polluted by other sources, and compensate with a M.C. simulation
   (d) Perform a second-order polynomial fit on the tail of the cumulative histogram, and subtract diffuse background
   (e) Compare the obtained distribution to other sources
4. Stack (weighted mean) all the obtained distributions.
5. Study PSF characteristics (statistics, containment radius), iterate from number *2.* to tune the parameters

Step 2 - Source analysis

1. Browse 3FGL catalog to list polluting sources near each candidate
2. For each candidate and each energy bin:
   (a) Do *step 1, 3.a)* to *3.d)*
   (b) Compare the distribution to the PSF
   (c) In case of statistically significant deviations, compute the extended flux and characterise its angular morphology
   (d) Otherwise, derive an upper bound on the extended flux from the measurement uncertainties
3. Build the energy spectrum. For each candidate and each energy bin:
   (a) Cut with `gtselect`, 1-2° f.o.v., 90° azimuthal angle.
   (b) Count the number of photons from source (`gtbin`, light curve, one time bin)
   (c) Compute the exposure with `gtexposure`
   (d) Remove background contribution
   (e) Check consistency with 2.a)

5 Results

We use the data from Fermi LAT Pass 8, P8R2 release. To maximise statistics, we choose to use the `source` class of events with both `front` and `back` events. The maximum zenith angle allowed for each event is 90°.
The events have been recorded from the start of Fermi operations on August the 4th, 2008, to May the 10th, 2016. This corresponds to 7 years, 10 months of data. The analysis is conducted over 8 logarithmically spaced energy bins, from 600 MeV to 50 GeV. The "Flux" appellation is often written as $E^2 \frac{dN}{dE}$ in the literature.
Source list and secondary figures are joined as appendix at the end of the document.

5.1 Point Spread Function

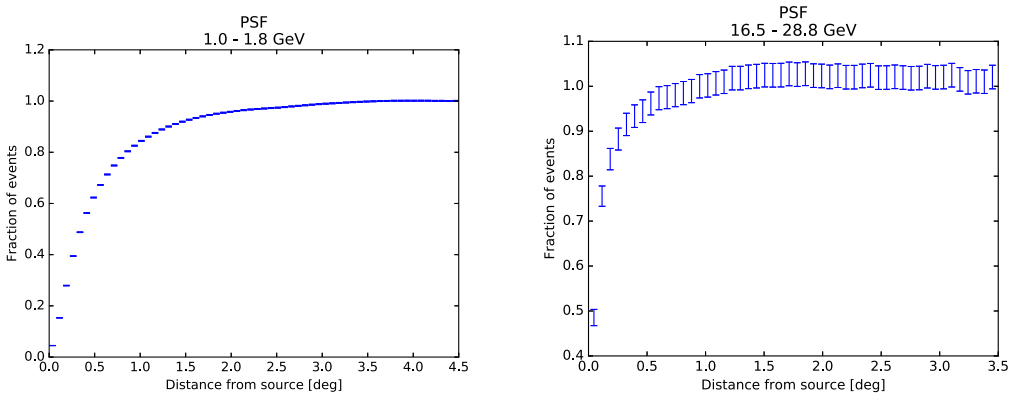

Figure 5.1 – *Experimental PSF in the 1-1.8 GeV and 16.5-28.8 GeV ranges.*

As a starting result we present on figure 5.1 the general appearance of our "experimental" PSF in the $\sim$ 1 GeV and $\sim$ 20 GeV areas. As the energy increases, the photon flux get lower which worsen the statistics. Indeed the PSF at 20 GeV has a considerably larger uncertainty, of the order of 7% whereas at 1 GeV the relative error is of the order of 1%. This already shows that detecting an extended emission will prove to be more difficult at higher energies as expected. In return as will be discussed below the PSF is considerably narrower in the 20 GeV range than in the 1 GeV range.
This PSF was built out of the selection process that we described previously. At

energies around 1 GeV, the Vela and Geminga pulsars are considerably brighter than other potential sources as shown in figure 5.2a where the raw photon count (without background) is compared between the different reference objects. Vela has twice the flux of Geminga, itself having roughly four times the flux from the Crab. This means that at low energy we will effectively be comparing the emission from potential candidates to the Vela and Geminga pulsars under the assumption that they can be treated as point sources. Figure 5.2b shows nevertheless that in the 1 GeV area their emissions are comparable. Indeed the cumulative photon distributions overlap each other after being normalised by their respective number of events. Having additional sources increase the accuracy by improving the statistics, but at 1 GeV the Vela and Geminga pulsars are so bright that they are almost sufficient to build an acceptable PSF.

As the energy grows the statistics worsen and we need to add additional sources. The PSF composition is shown in figure 5.2c between 5.5 and 9.5 GeV as an example: the uncertainties get wider and we add an additional point source (here quasar PKS B1424-418) with a photon distribution still compatible with that of the three main pulsars.

The PSF is expected to get wider at lower energy and narrower at higher energy. We report on figure 5.3 its evolution. We see indeed in 5.3a that at below 1 GeV the cumulative distribution is considerably broader than above 10 GeV. In the 600 MeV - 1 GeV energy bin, the distribution flattens as far as 3.0° away from the source, meaning that there are still photons counted at that distance. As the energy increases the source gets more "point-like" with a narrower curve.

An important criteria to evaluate how broad the PSF is is the *68% containment radius* (CR), i.e. the angular radius at which 68% of the photons are counted. We report its evolution in figure 5.3b. The 68% CR evolves following a power-law below $\sim$ 10 GeV and gets constant afterwards. At 1 GeV it reaches a radius as big as 1.0°, twice the angular size of the Moon. At that point any potential extended emission or diffuse halo is likely to be "hidden" inside of the PSF and hence contribute to the point-source flux. Due to this result we choose not to explore energies lower than 600 MeV despite the Fermi ability to go below 100 MeV, and treat with caution any result below 1 GeV.

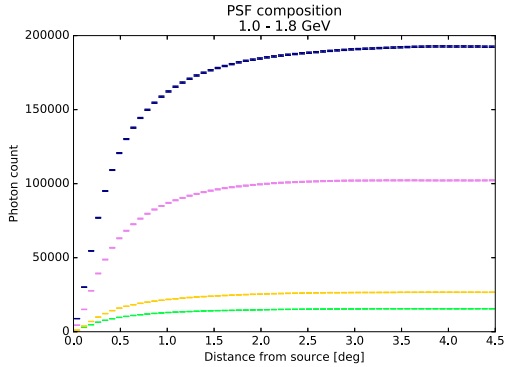

(a) *Photon distribution at 1-1.8 GeV.*

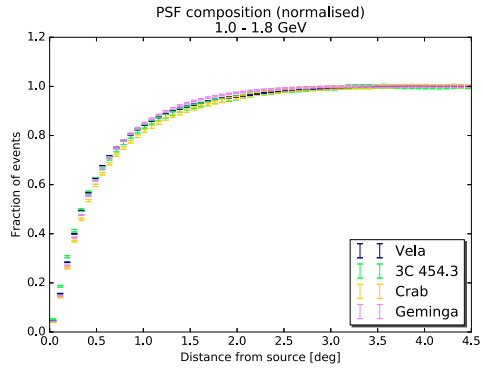

(b) *Normalised distribution at 1-1.8 GeV*

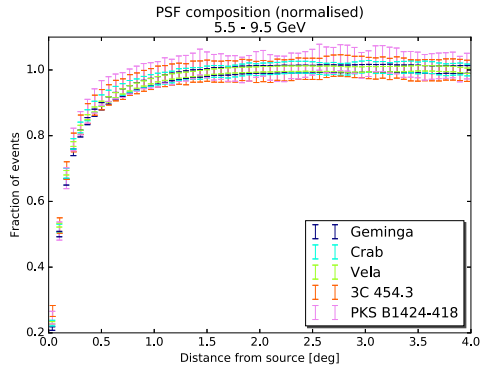

(c) *Normalised distribution at 5.5-9.5 GeV*

Figure 5.2 – *Experimental Point Spread Functions components. Angular distributions show the dominant contributions to the PSF, and normalised graphs compare their shapes. The same legend applies for side-by-side graphs.*

The 95% CR, the radius where almost all photons are counted, was found by both the Fermi LAT team and the present study to be roughly three times the 68% CR. Again this means that some emissions from point sources can be reconstructed over an area of 3.0° below 1 GeV.

On figure 5.3b we added a dashed line at 0.15°. This value is used in the analysis to determine the cut radius around secondary polluting sources, above 10 GeV.

Care must be taken when choosing the energy binning. This wide, power-law decreasing PSF can introduce some bias in the flux measurements: suppose we study an object with a soft spectrum over a bin as wide as 1-10 GeV. Due to the spectral characteristics there will be an excess of photons at the lower end of that bin. The bias is reversed with a hard spectrum, where the excess will show on the higher end. Energy bins must hence be narrow enough to take that effect into

account while still being wide enough to have acceptable statistics. Pulsars are actually good sources to build a PSF due to their relatively flat spectrum.

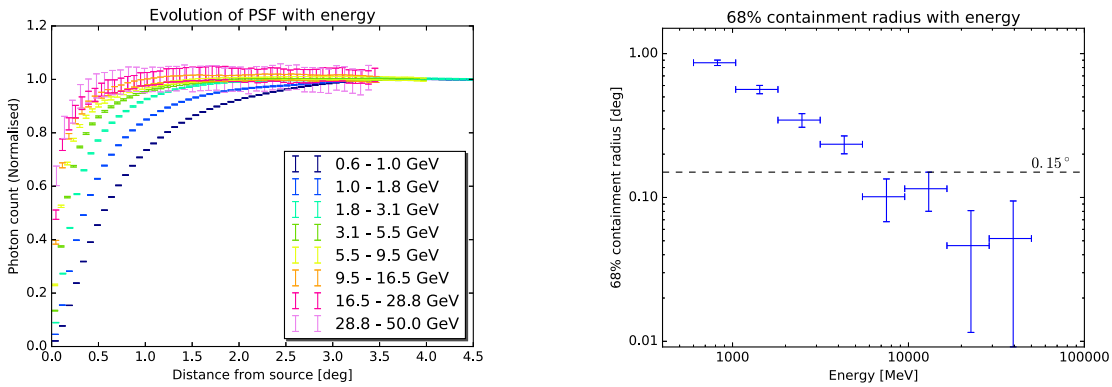

(a) Photon angular distribution at different energies.

(b) Power-law evolution of the 68% containment radius.

Figure 5.3 – *Evolution of the experimental PSF from 600 MeV to 50 GeV.*

5.2 Pulsar spectra

As a test of the analysis method we measure the spectra from the three main pulsars. We report the results for Vela and Geminga in figure 5.4 and for the Crab in figure 5.5.

Vela and Geminga show a quite high energy flux: again these two objects are relatively close to the Earth which strongly increase their magnitude in comparison to other objects in the gamma ray sky. Their flux is relatively flat below 5 GeV and drops sharply above $\sim$ 10 GeV. This is the known cut-off of pulsars spectra. Vela is not even detected above 30 GeV: over the 8 years of observation only 4 ± 6 photons were detected in a radius of 1.0° around the pulsar. These spectral features and values are consistent with the official LAT observations[4][5]. They reconfirm again that at energies above $\sim$ 7-10 GeV additional point sources are needed to build an accurate PSF.

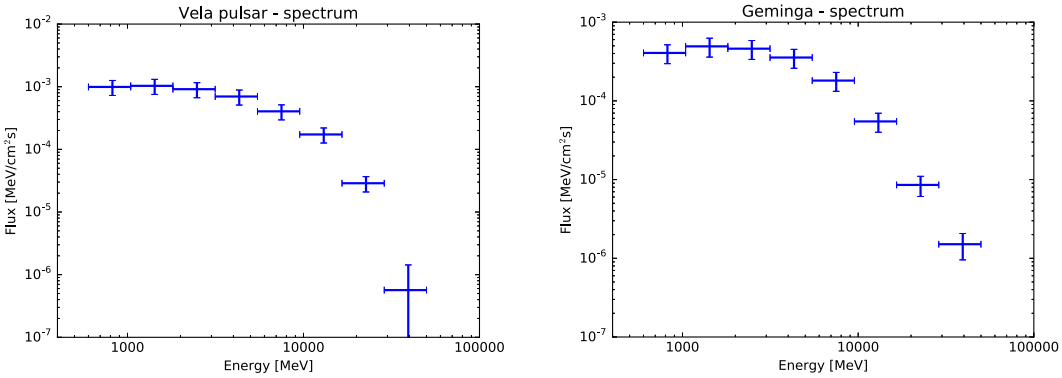

Figure 5.4 – *Energy spectra for the Vela pulsar (left) and Geminga (right) in log/log scale. Signal from Vela is not significant above 30 GeV, with* 4 ± 6 *photons detected in 8 years.*

The Crab spectrum shows a steady decrease in energy flux following a power law up to $\sim$ 50 GeV, at which point the energy spectrum rises again. This is a priori unexpected as a cut-off would be expected in the 10 GeV area. However the Crab pulsar lies within its supernova remnant: due to how young it is (one millennium) the forming nebula is still quite bright and relatively small: of the order of 0.05°. This nebula features a spectral peak at $\sim$ 100 GeV which is observed in figure 5.5. This result is therefore consistent with other observations[6] in the assumption that above 10 GeV our analysis is catching the nebula emission instead of the pulsar. Due to the Crab nebula having a smaller angular size than the Fermi LAT resolution, it can be used as a reference PSF above $\sim$ 30 GeV.

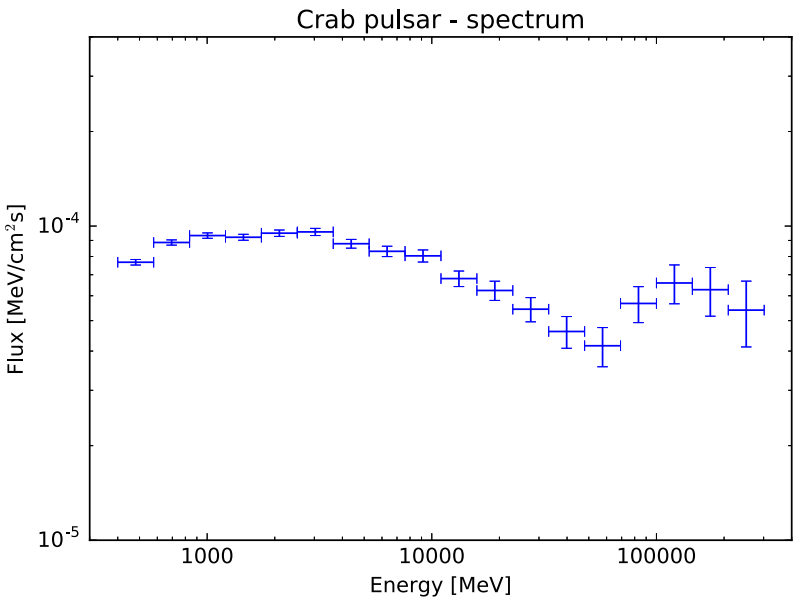

Figure 5.5 – *Energy spectrum for the Crab pulsar from 400 MeV to 300 GeV.*

5.3 Blazar study

5.3.1 Markarian 421

Markarian 421 (Mrk421) is one of the brightest BL Lac objects in the sky due to its low redshift. It is therefore a perfect object to test the method and get some first results.

The angular photon distribution showed no difference between the PSF and Mrk421. Hence no extended emission was detected. However the respective statistics can still lead to upper bounds on the halo flux that can be compared to the theory.

We report in figure 5.6 the full results from the study on Mrk421. Data points labelled as *energy flux* were obtained using aperture photometry on Fermi LAT data. The spectrum is extended thanks to the measurement of the *MAGIC* Cherenkov telescope: both data set seem in agreement with each other as they connect at the same flux at 300 GeV. Finally *Upper bounds* refer to the maximum possible difference between our PSF and the angular distribution, at a distance of 1.0°.

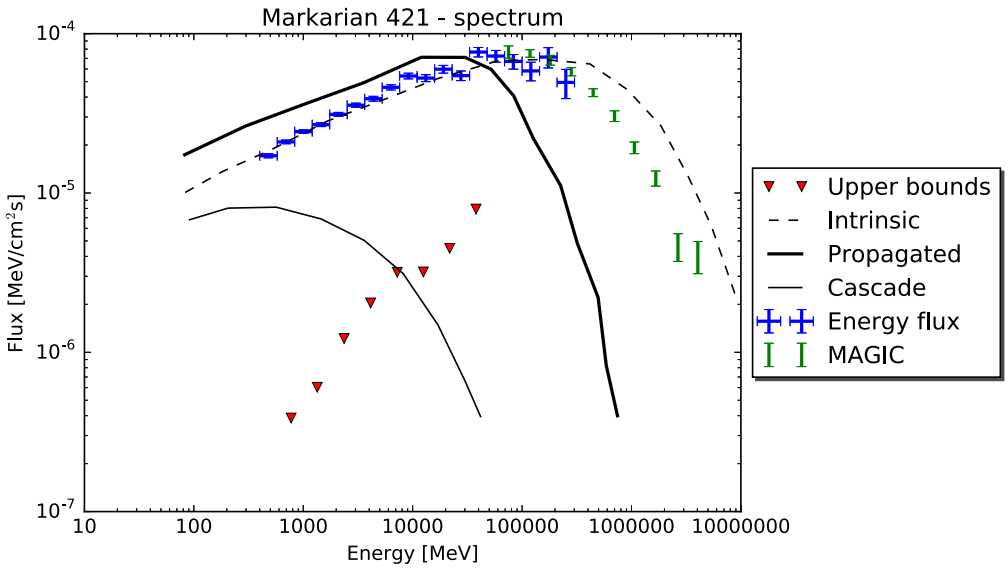

Figure 5.6 – *Markarian 421 spectrum. Blue points from Fermi LAT (400 MeV - 300 GeV), red points bounds on extended emission (Fermi LAT, 600 MeV - 50 GeV), green points from MAGIC.*

Three theoretical curves are joined to the graph[32]. *Intrinsic* refers to the source original flux. It is modelled as a power law with a cut-off at 1 TeV. *Cascade* is the hypothetical halo flux under the assumption of a null magnetic field. *Propagated* is the measured flux, taking into account the intrinsic flux with the interactions with the extragalactic background light and the cascade contribution.
Our upper bounds are not compatible with a null magnetic field as the data points on figure 5.6 are below the "Cascade" curve. The halo must therefore be suppressed in the 1-10 GeV range. We also note that in the 1 GeV area there is a factor 10^2 between the energy flux and the maximum possible extended emission.
The data is consistent with a cut-off in the TeV area. An extended emission above 20-30 GeV is therefore extremely unlikely as there will be a lack of very high energy photons to produce cascades with such kind of energies. The observed cut-off appears moreover at slightly lower energy than what the "Intrinsic" model predicts: the high energy flux must therefore be suppressed on its way to the Earth, likely by interaction with the extragalactic background light. However the flux is not as suppressed as what the "Propagated" model suggests, which is due

to the overestimate of the halo flux that we mentioned previously.
Using equation 1.2 in the limit of large correlation lengths, we can derive bounds on the cosmological magnetic field. For Mrk421 due to its proximity we approximate the optical depth τ to 1 and the redshift z to 0.
At an energy of 1 GeV, if $B \lesssim 5 \cdot 10^{-17}$ G the expected extended emission is smaller than 0.8°, which is of the order of the 68% CR of the PSF. Hence at that level the halo will not be detected as its emission is mixed with that of the blazar and contributes to the point source flux.
If $5 \cdot 10^{-17}$ G $\lesssim B \lesssim\sim 3 \cdot 10^{-15}$ G then the cascade flux is diluted by a factor of less than 10^2 and we should have observed it at the 1 GeV level. Since this is not the case, we finally conclude that $0 < B \lesssim 5 \cdot 10^{-17}$ G or $B \gtrsim 3 \cdot 10^{-15}$ G.

5.3.2 Markarian 501

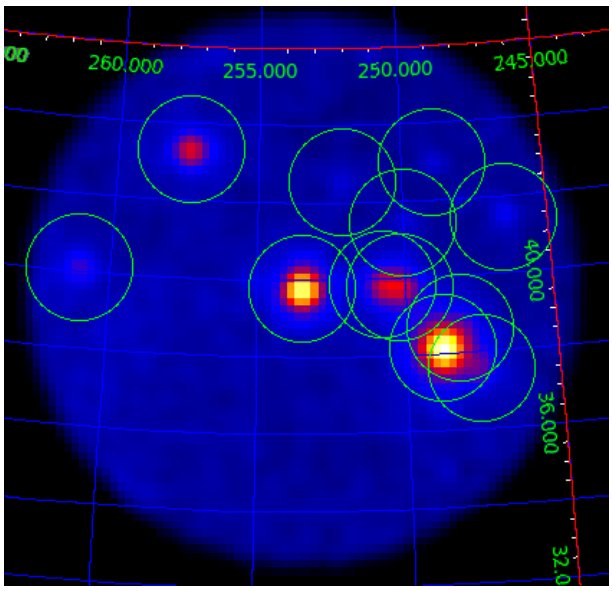

Figure 5.7 – *7° f.o.v count map around Markarian 501, 1.8-3.1 GeV. Green circles show the 95% containment radius (1.38°) around 3FGL sources. Horizontal axis is right ascension, vertical is declination. Mrk501 is the bright central object.*

Markarian 501 (Mrk501) is another low redshift BL Lac object that might provide interesting results. It has however a considerable complication: a 7° field

of view image around that blazars reveals a crowded neighbourhood. Two 3FGL catalogued sources are within 3° of Mrk501, plus additional objects further away. A significant problem at low energies is the PSF width: the emission from Mrk501 can overlap with the flux from one of its neighbour. In figure 5.7 we show a count map between 1.8 and 3.1 GeV, with the 95% CR of each polluting source represented as a circle. In that energy range there is already considerable overlap at the scales where one would expect to find an extended emission. Moreover the PSF widens exponentially when energy decreases. It is therefore impossible to probe for diffuse halos at energies below ~ 2 GeV without additional techniques.

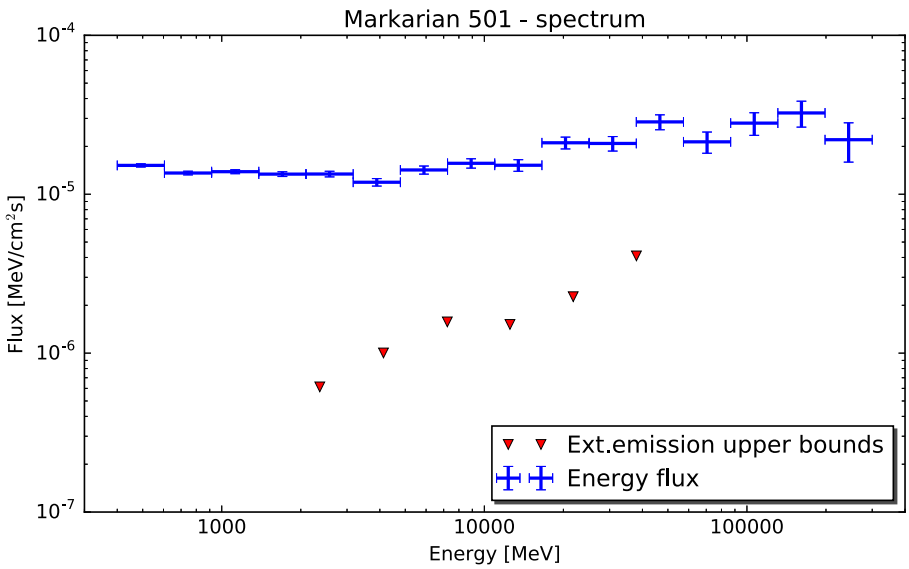

Figure 5.8 – *Energy spectrum of blazar Markarian 501 from 400 MeV to 300 GeV (16 bins), with bounds on extended emission from 1.8 to 50 GeV (6 bins).*

At an energy of 5 GeV and assuming $\tau = 1$, if the magnetic field $B \lesssim 10^{-16}$ G the angular size of the halo would be at the level of 0.7° and cannot therefore be distinguished from the source flux due to the wide PSF. If $B \lesssim 10^{-15}$ G the extended emission is diluted by a factor of less than 10 and we should have observed it at 5 GeV. We can therefore exclude values between 10^{-16} and 10^{-15} G.
TeV measurements show a cut-off around 10 TeV[38] which is higher than Markarian 421. Hence Mrk501 would be a better candidate for extended emissions. It

is however difficult to extend figure 5.8 as there are currently no reports of the baseline flux in TeV range.

5.3.3 PKS 1424+240

This blazar is much further away than the two previous ones with an uncertain redshift of 0.88 ± 0.28. As such it is considerably fainter on the sky.
The angular emission from PKS 1424 is overall consistent with the PSF with a notable exception between 1.8 and 3.1 GeV where a small difference can be seen. The cumulative plots are shown in figure 5.9a. A small shift can be observed between 0.5° and 1.0°. Figure 5.9b show the difference between both distributions and we indeed notice a non-zero difference which is inconsistent with the uncertainties.
This result is however of low significance. First the difference is of the order of 1.5 σ which is consistent with a statistical fluctuation. Moreover figure 5.9a reveals that the background treatment was not completely effective as there is a small bump at 2.5° and additional fluctuations at 3.5°. This would typically be caused by a polluting gamma ray source. The 3FGL catalogued objects around PKS 1424 are shown in figure 2.6 and were all taken into account during the analysis, yet one signal went through.
Figure 5.10 shows the energy spectrum of PKS 1424+240 using the same quantities and notation as for Markarian 421 previously.

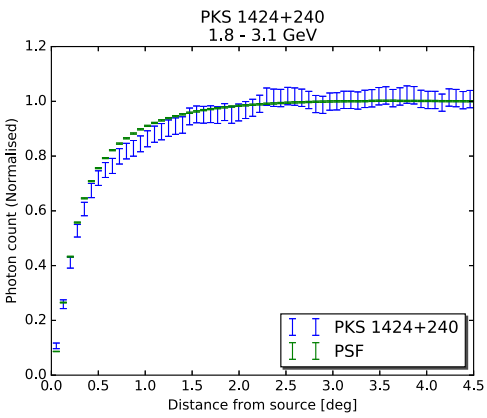

(a) Normalised photon angular distribution compared to the PSF.

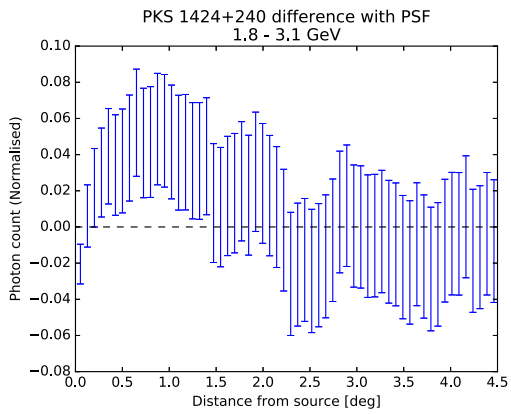

(b) Difference between the normalised distribution and the PSF.

Figure 5.9 – *PKS 1424+240 photon distribution, 1.8-3.1 GeV, showing an extended emission in the 0.5° - 1.0° area with a* $\sim 1.5\sigma$ *significance.*

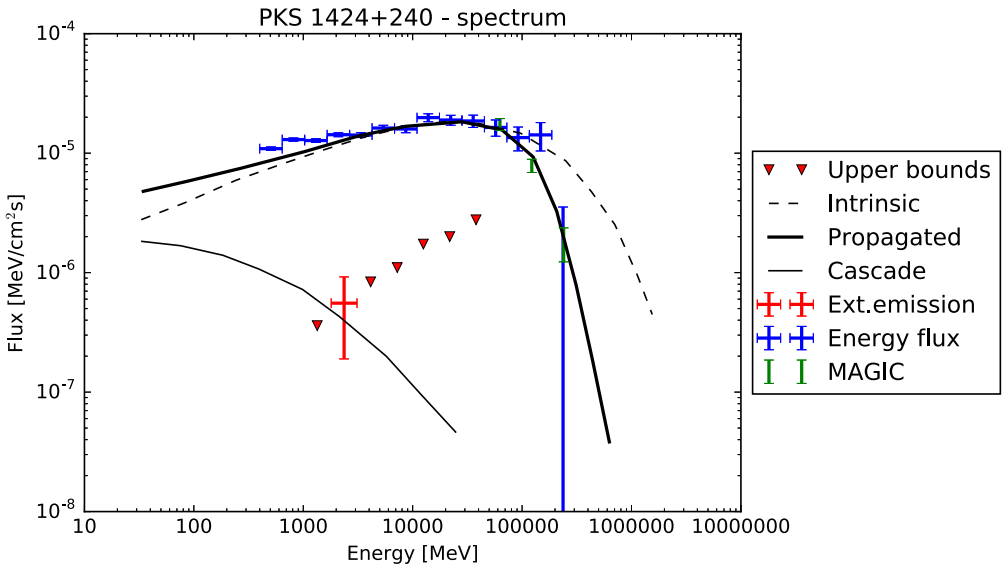

Figure 5.10 – *PKS 1424+240 spectrum. Blue points from Fermi LAT (400 MeV - 300 GeV), red points bounds on extended emission (Fermi LAT, 1 - 50 GeV), green points from MAGIC. Detection of extended emission in the 1.8 - 3.1 GeV.*

Data points labelled as energy flux were obtained using aperture photometry on Fermi LAT data. The "intrinsic" curves refers to the source spectrum with a cut-off at 1 TeV, "cascade" is the hypothetical flux given no magnetic field and "propagated" is the measured flux after the cascade.
The spectrum seems more or less in agreement with MAGIC data with the exception of the two last LAT points: the curve seems first to follow the intrinsic curve while MAGIC follows the propagated. The final point is well below the 10^{-8} MeV/cm^{2}s as the aperture photometry only picked a single event between 28.8 and 50 GeV in a 2.5° radius around the blazar in 8 years. In other words, the source was not detected above $\sim$ 28.0 GeV. At lower energies, the flux is consistent with the "propagated" model implying no suppression of the magnetic field.
The upper bounds on extended emission do not put constraints the magnetic field: all points above 3 GeV show an upper limit higher than the "cascade" flux. The detection is consistent with the "cascade". Only one point lies below the curve, but it is not sufficiently different to claim a significant result.
At 1 GeV, given an optical depth of $\tau = 10$ and a redshift $z = 0.88$ (uncertain),

if the magnetic field is weaker than $5 \cdot 10^{-16}$ G the expected angular size of the extended emission is lower than 0.7° and can therefore be hidden inside the PSF. The models presented here however suppose a cut-off at 1 TeV. If the source flux goes beyond we can expect a more important halo emission in the GeV range. Current instruments such as Fermi and MAGIC are not able to locate that cut-off: either due to the Fermi's energy bounds or due to MAGIC low sensitivity to far away sources. Upcoming detectors such as the Cherenkov Telescope Array (CTA) may improve the models and allow for tighter constraints.

Note on 1ES 0229+200

1ES 0229+200 is a quite distant and faint blazar located near the galactic plane. It has however a hard spectrum and is actually quite bright in TeV range. It is therefore one of the prime candidates for extended emissions and for direct measurements of the magnetic field. In particular it has allowed to derive lower bounds on the extragalactic magnetic field strength[45].
However this blazar is very faint in the 1 - 50 GeV range probed by our analysis and we were not able to get a significant photon angular distribution or even a detection. Further improvement of the method might yield better results which could be cross-checked with the next generation of gamma ray telescopes.

6 Conclusion

The purpose of this work was to look for extended emissions around TeV-class blazars by using data from the Fermi gamma ray space telescope, motivated by the study of cosmic extragalactic magnetic fields.
From a set of pulsars and radio quasars we successfully built a point spread function to use as a reference in further analysis and noted the very wide containment radius at energies below 1 GeV. We concluded that below 500-600 MeV the PSF was too wide to accurately probe for halo and diffuse emissions. The containment radius improves exponentially down to $0.1°$ at 10 GeV and above.
The analysis method was successfully tested on pulsars spectra, yielding results consistent with other studies. We noted that pulsar spectra feature a sharp cut-off at 10 GeV which reduces their use as reference point sources at high energy.
Bounds for an extended emission were derived for blazar Markarian 421, placing the halo flux at less than 1% of the source flux at 1 GeV. This result is inconsistent with a lack of extragalactic magnetic field. We excluded values for the field strength between $5 \cdot 10^{-17}$ G and $3 \cdot 10^{-15}$ G.
A consistent yet narrower exclusion zone was derived from Markarian 501. The blazar is a potentially interesting candidate due to its hard spectrum but further measurements in the TeV range are needed.
Hints of an extended emission at the $\sim 1.5\sigma$ level were found at 2-3 GeV around PKS 1424+240. The low significance of this result and the possibility of it being caused by a failure in the noise treatment didn't permit any conclusion. Upper bounds for the extended emission were derived, placing the halo flux at less than 5% of the source flux at 3 GeV. The bounds were consistent with a model of zero magnetic field, but the model can be improved if further measurements with next-generation Cherenkov telescopes detect a higher energy cut-off.
No measurements were performed on 1ES 0229+200. The current analysis method didn't yield any exploitable result due to how faint the source is and the significant diffuse component in that area of the sky. Further improvements of the current method alongside measurement from next generation Cherenkov telescopes could allow studies of 1ES 0229+200 flux and potential halo. The current analysis can nevertheless be applied to a variety of low-to-high redshift blazars to probe for extended emissions.

Acknowledgement

The author would like to thank:

- Prof. Dr. Aurelio Bay, Prof. Dr. Andrii Neronov for their guidance and advice during this work.
- The NASA Goddard Space Flight Center, for launching and operating the Fermi space telescope and releasing data to the public.
- Cyril Alispach for the constant collaboration and good laughs shared.
- My parents and brother for the unshakeable moral support provided.

References

[1] Abdo, A. A., et al. "Spectrum of the isotropic diffuse gamma-ray emission derived from first-year fermi large area telescope data." *Physical Review Letters* 104.10 (2010): 101101.

[2] Abdo, A. A., et al. "The Fermi gamma-ray space telescope discovers the pulsar in the young galactic supernova remnant CTA 1." *Science* 322.5905 (2008): 1218-1221.

[3] Abdo, A. A., et al. "Fermi observations of GRB 090902B: a distinct spectral component in the prompt and delayed emission." *The Astrophysical Journal Letters* 706.1 (2009): L138.

[4] Abdo, A. A., et al. "The Vela pulsar: results from the first year of Fermi LAT observations." *The Astrophysical Journal* 713.1 (2010): 154.

[5] Abdo, A. A., et al. "Fermi-LAT observations of the Geminga pulsar." *The Astrophysical Journal* 720.1 (2010): 272.

[6] Abdo, A. A., et al. "Fermi Large Area Telescope observations of the Crab pulsar and nebula." *The Astrophysical Journal* 708.2 (2009): 1254.

[7] Ackermann, M., et al. "Determination of the point-spread function for the Fermi large area telescope from on-orbit data and limits on pair halos of active galactic nuclei." *The Astrophysical Journal* 765.1 (2013): 54.

[8] Aharonian, F., et al. "New constraints on the mid-IR EBL from the HESS discovery of VHE *gamma*-rays from 1ES 0229+ 200." *Astronomy & Astrophysics* 475.2 (2007): L9-L13.

[9] Aharonian, F. A., P. S. Coppi, and H. J. Völk. "Very High Energy Gamma-Rays from AGN: Cascading on the Cosmic Background Radiation Fields and the Formation of Pair Halos." *arXiv preprint astro-ph/9312045* (1993).

[10] Alonso, Mateo Fernandez. "Search for extended gamma ray emission in Markarian 421 using VERITAS observations." *arXiv preprint arXiv:1406.4764* (2014).

[11] Antonucci, Robert. "Unified models for active galactic nuclei and quasars." Annual review of astronomy and astrophysics 31 (1993): 473-521.

[12] Atwood, W. B., et al. "Design and initial tests of the Tracker-converter of the Gamma-ray Large Area Space Telescope." *Astroparticle Physics* 28.4 (2007): 422-434.

[13] Atwood, W. B., et al. "The large area telescope on the Fermi gamma-ray space telescope mission." *The Astrophysical Journal* 697.2 (2009): 1071.

[14] Band, D. L., and E. Ferrara. "Fermi Gamma-ray Telescope–Cicerone: Detailed Manual for Fermi Science Tools." (2009): 107.

[15] Beck, Rainer. "Galactic and extragalactic magnetic fields." *arXiv preprint astro-ph/0012402* (2000).

[16] Durrer, Ruth, and Andrii Neronov. "Cosmological magnetic fields: their generation, evolution and observation." *The Astronomy and Astrophysics Review* 21.1 (2013): 1-109.

[17] Fornasa, Mattia, and Miguel A. Sanchez-Conde. "The nature of the diffuse gamma-ray background." *Physics Reports* 598 (2015): 1-58.

[18] Gaidos, J. A., et al. "Extremely rapid bursts of TeV photons from the active galaxy Markarian 421." (1996): 319-320.

[19] Gehrels, Neil, et al. "The Swift gamma-ray burst mission." *The Astrophysical Journal* 611.2 (2004): 1005.

[20] Ghisellini, G., and F. Tavecchio. "The blazar sequence: a new perspective." Monthly Notices of the Royal Astronomical Society 387.4 (2008): 1669-1680.

[21] Gondolo, Paolo, and Joseph Silk. "Dark matter annihilation at the galactic center." *Physical Review Letters* 83.9 (1999): 1719.

[22] Gould, Robert J., and Gerald Schréder. "Opacity of the universe to high-energy photons." *Physical Review Letters* 16.6 (1966): 252.

[23] Hauser, Michael G., and Eli Dwek. "The cosmic infrared background: measurements and implications." *arXiv preprint astro-ph/0105539* (2001).

[24] Hektor, Andi, Martti Raidal, and Elmo Tempel. "Fermi-LAT gamma-ray signal from Earth Limb, systematic detector effects and their implications for the 130 GeV gamma-ray excess." *The European Physical Journal C* 73.10 (2013): 1-9.

[25] Hinton, James Anthony, and HESS collaboration. "The status of the HESS project." *New Astronomy Reviews* 48.5 (2004): 331-337.

[26] King, Ivan. "The structure of star clusters. I. An empirical density law." *The Astronomical Journal* 67 (1962): 471.

[27] Johnson, W. N., et al. "A CsI (Tl) hodoscopic calorimeter for the GLAST mission." *Nuclear Science Symposium*, 1997. IEEE. IEEE, 1997.

[28] Lorenz, Eckart, and MAGIC collaboration. "Status of the 17 m∅ MAGIC telescope." *New Astronomy Reviews* 48.5 (2004): 339-344.

[29] Meegan, Charles, et al. "The Fermi gamma-ray burst monitor." *The Astrophysical Journal* 702.1 (2009): 791.

[30] NASA Goddard Space Flight Center. "Fermi Science Support Center". *Nasa: Fermi Gamma-ray Space Telescope*. http://fermi.gsfc.nasa.gov/ssc/. Retrieved 20 February 2016.

[31] NASA Goddard Space Flight Center. "NASA - Q& A ON THE GLAST MISSION". *Nasa: Fermi Gamma-ray Space Telescope*. 28 August 2008. Retrieved 12 June 2016.

[32] Neronov, A., and D. V. Semikoz. "Sensitivity of γ-ray telescopes for detection of magnetic fields in the intergalactic medium." *Physical Review* D 80.12 (2009): 123012.

[33] Neronov, Andrii, and Ievgen Vovk. "Evidence for strong extragalactic magnetic fields from Fermi observations of TeV blazars." *Science* 328.5974 (2010): 73-75.

[34] Neronov, A. "Introduction to astroparticle physics". Lecture at EPFL. (2016)

[35] Nolan, P. L., et al. "Fermi Large Area Telescope Second Source Catalog" *The Astrophysical Journal Supplement Series* 199.2 (2012): 31.

[36] N2YO. *GLAST Satellite details 2008-029A NORAD 33053*. http://www.n2yo.com/satellite/?s=33053. Consulted: February 2016.

[37] Ritz, S., and GLAST Mission Team. "Overview of the GLAST Mission and Opportunities." *The First GLAST Symposium.* Vol. 921. No. 1. AIP Publishing, 2007.

[38] Samuelson, F. W., et al. "The TeV Spectrum of Markarian 501." *The Astrophysical Journal Letters* 501.1 (1998): L17.

[39] Selig, Marco, et al. "The denoised, deconvolved, and decomposed Fermi γ-ray sky-An application of the D3PO algorithm." *Astronomy & Astrophysics* 581 (2015): A126.

[40] S. Swordy, "The energy spectra and anisotropies of cosmic rays". *Space Science Reviews* 99, pp.85–94. (2001)

[41] Su, Meng, Tracy R. Slatyer, and Douglas P. Finkbeiner. "Giant gamma-ray bubbles from Fermi-LAT: active galactic nucleus activity or bipolar galactic wind?." *The Astrophysical Journal* 724.2 (2010): 1044.

[42] Tavani, M., et al. "The AGILE mission." *Astronomy & Astrophysics* 502.3 (2009): 995-1013.

[43] Taylor, A. M., Ie Vovk, and A. Neronov. "Extragalactic magnetic fields constraints from simultaneous GeV–TeV observations of blazars." *Astronomy & Astrophysics* 529 (2011): A144.

[44] Urry, C. Megan. "AGN Unification: An Update." *arXiv preprint astro-ph/0312545* (2003).

[45] Vovk, Ie, et al. "Fermi/LAT observations of 1ES 0229+ 200: implications for extragalactic magnetic fields and background light." *The Astrophysical Journal Letters* 747.1 (2012): L14.

[46] Wakely, S. P., and D. Horan. "TeVCat: An online catalog for Very High Energy Gamma-Ray Astronomy." *International Cosmic Ray Conference.* Vol. 3. 2008.

[47] Weekes, T. C., et al. "VERITAS: the very energetic radiation imaging telescope array system." *Astroparticle Physics* 17.2 (2002): 221-243.

[48] Winkler, Christoph, et al. "The INTEGRAL mission." *Astronomy & Astrophysics* 411.1 (2003): L1-L6.

[49] Woosley, S. E., and J. S. Bloom. "The Supernova–Gamma-Ray Burst Connection." *arXiv preprint astro-ph/0609142* (2006).

[50] Woosley, Stan, and Thomas Janka. "The physics of core-collapse supernovae." *Nature Physics* 1.3 (2005): 147-154.

[51] Zhang, Bin-Bin, et al. "A comprehensive analysis of Fermi gamma-ray burst data. I. Spectral components and the possible physical origins of LAT/GBM GRBs." *The Astrophysical Journal* 730.2 (2011): 141.

A Appendices

A.1 Abbreviation table

3 FGL	Third Fermi Gamma-ray LAT point sources catalog
AGN	Active Galactic Nuclei
BL Lac	BL Lacertae object, type of AGN
C.R.	Containment Radius
DGRB	Diffuse Gamma-Ray Background
e^+, e^-	positron, electron
eV	electron-Volt ($1.6021 \cdot 10^{-19}$ Joules)
fov	Field of view
FSRQ	Flat Spectrum Radio Quasar
GRB	Gamma-Ray Burst
LAT	Large Area Telescope
M.C.	Monte-Carlo
Mrk421, Mrk501	Markarian 421, Markarian 501
RA, Dec	Right Ascension, Declination (equatorial coordinates, J2000)
PSF	Point Spread Function
PSR	Pulsar

A.2 Source list

Name	**RA** [deg]	**Dec** [deg]	**Type**	**Used for**
Vela pulsar	128.836	-45.1764	Pulsar	PSF
Geminga	98.4788	17.7732	Pulsar	PSF
Crab pulsar	83.6372	22.0241	Pulsar	PSF
CTA 1	1.7656	73.0499	Pulsar	PSF
3C 454.3	343.5018	16.1459	FSRQ	PSF
PKS B1424-418	216.9914	-42.1106	FSRQ	PSF
Markarian 421	166.114	38.2088	BL Lac	Candidate
Markarian 501	253.468	39.7602	BL Lac	Candidate
PKS 1424+240	216.752	23.8	BL Lac	Candidate
1ES 0229+200	38.2026	20.2882	BL Lac	Candidate

Table A.1 – *Sources of interest.*

Energy range (GeV)	**Source list**
0.6 - 1.0	Vela, Geminga, Crab
1.0 - 1.8	Vela, Geminga, Crab, 3C 454.3
1.8 - 3.1	Vela, Geminga, Crab, 3C 454.3
3.1 - 5.5	Vela, Geminga, Crab, 3C 454.3
5.5 - 9.5	Vela, Geminga, Crab, PKS B1424-418, 3C 454.3
9.5 - 16.5	Vela, Geminga, Crab, CTA 1, PKS B1424-418, 3C 454.3
16.5 - 28.8	Vela, Geminga, Crab, CTA 1, PKS B1424-418, 3C 454.3
28.8 - 50.0	Crab nebula

Table A.2 – *PSF composition.*

A.3 Additional plots

PSF composition

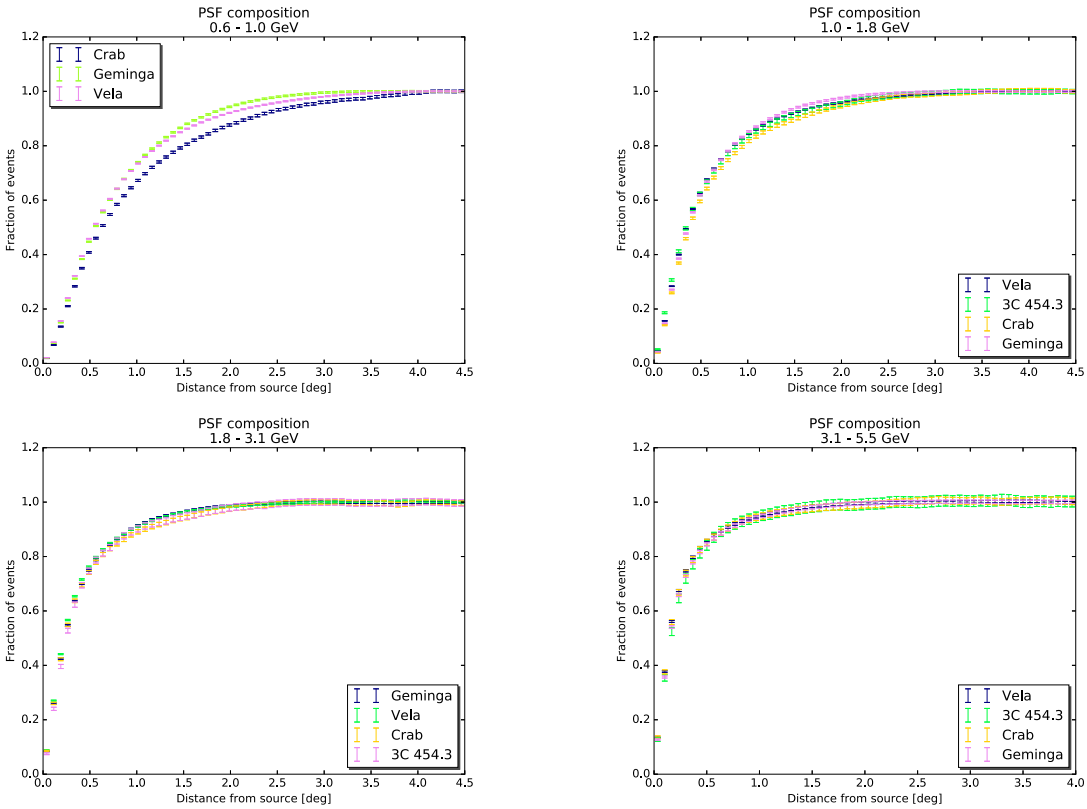

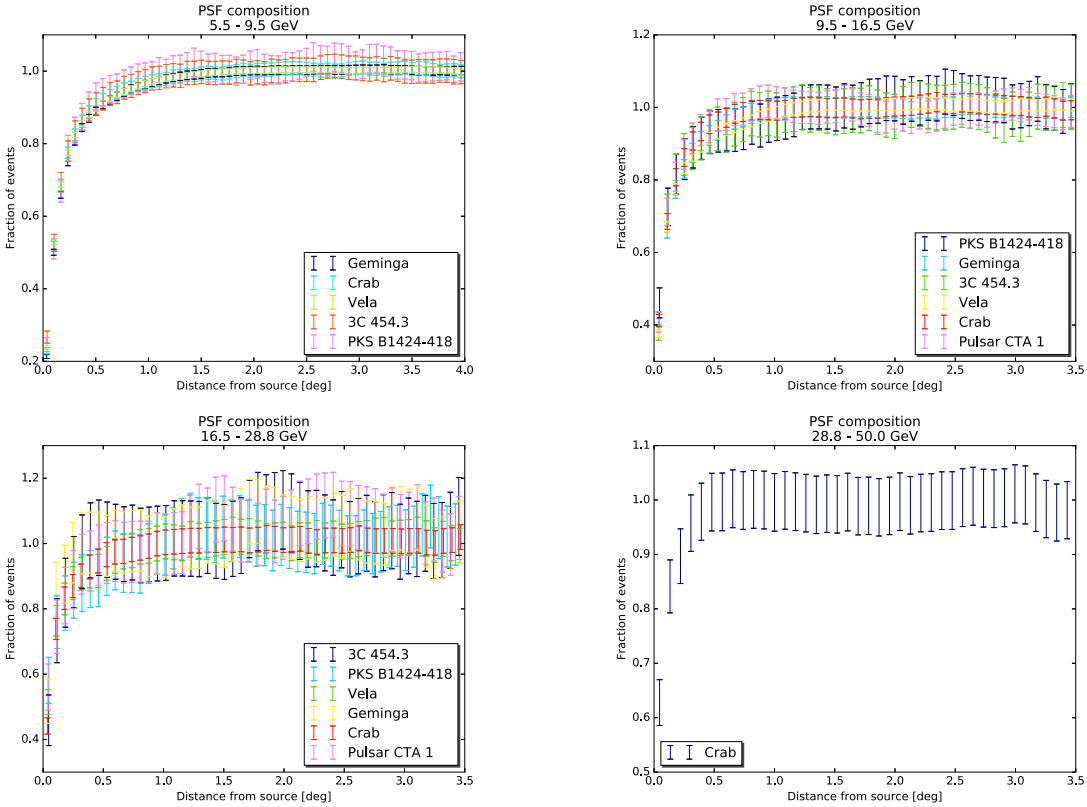
PSF composition
5.5 - 9.5 GeV
Fraction of events
Distance from source [deg]
Geminga
Crab
Vela
3C 454.3
PKS B1424-418
PSF composition
9.5 - 16.5 GeV
Fraction of events
Distance from source [deg]
PKS B1424-418
Geminga
3C 454.3
Vela
Crab
Pulsar CTA 1
PSF composition
16.5 - 28.8 GeV
Fraction of events
Distance from source [deg]
3C 454.3
PKS B1424-418
Vela
Geminga
Crab
Pulsar CTA 1
PSF composition
28.8 - 50.0 GeV
Fraction of events
Distance from source [deg]
Crab

Diffuse background fit

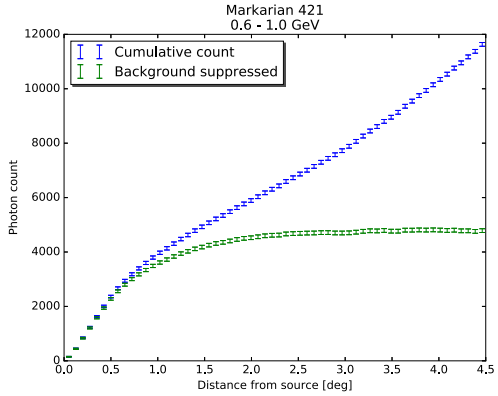

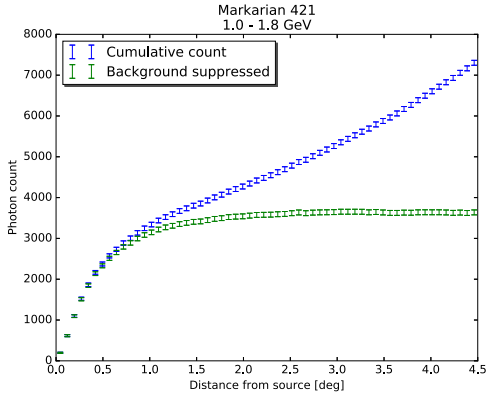

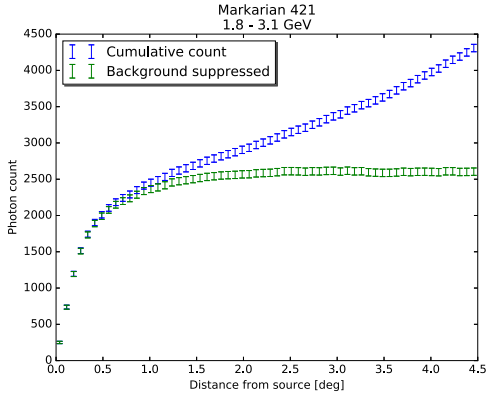

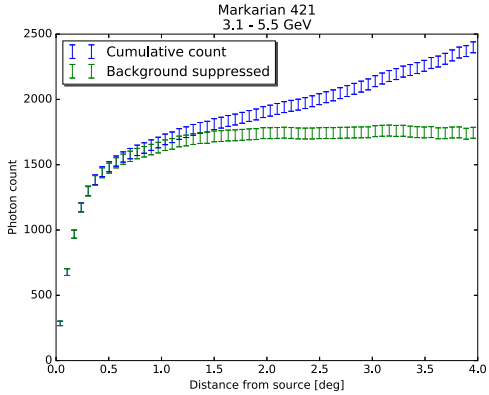

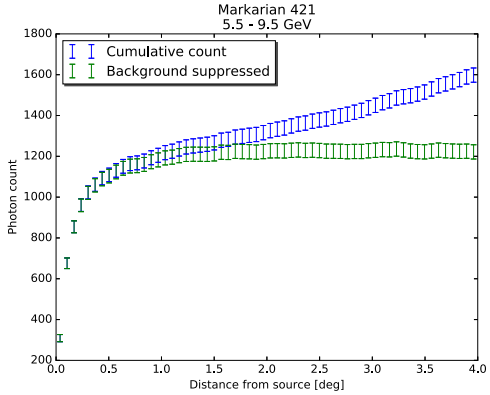

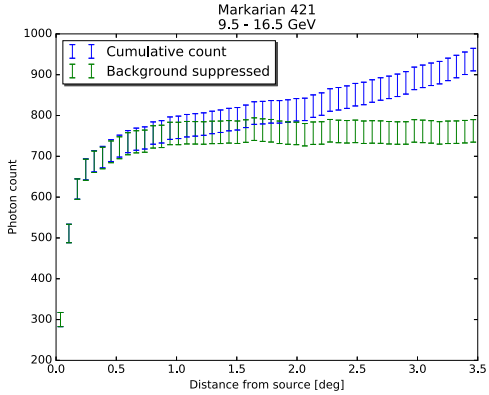

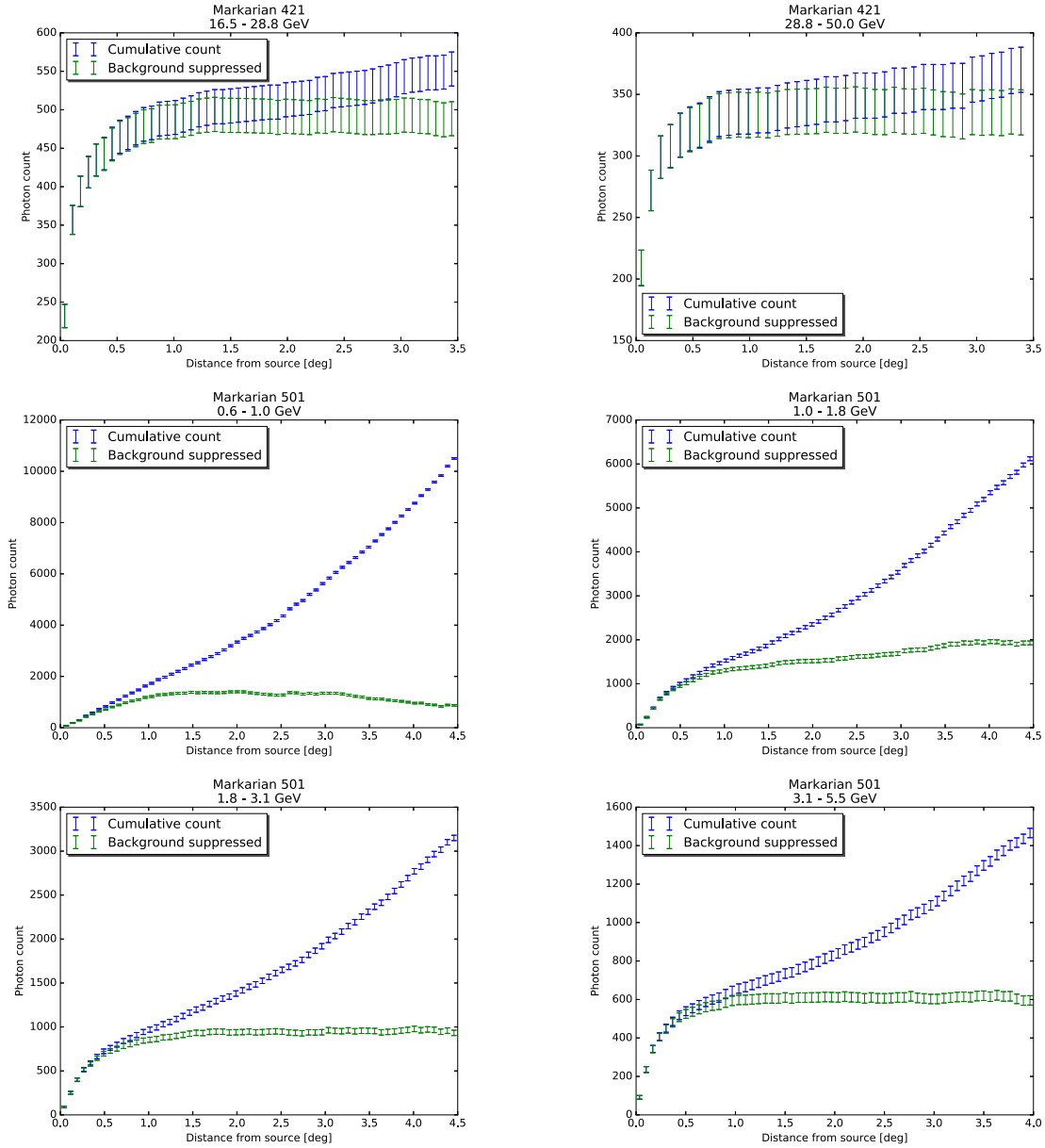
Markarian 421
16.5 - 28.8 GeV
Cumulative count
Background suppressed
Photon count
Distance from source [deg]
Markarian 421
28.8 - 50.0 GeV
Cumulative count
Background suppressed
Photon count
Distance from source [deg]
Markarian 501
0.6 - 1.0 GeV
Cumulative count
Background suppressed
Photon count
Distance from source [deg]
Markarian 501
1.0 - 1.8 GeV
Cumulative count
Background suppressed
Photon count
Distance from source [deg]
Markarian 501
1.8 - 3.1 GeV
Cumulative count
Background suppressed
Photon count
Distance from source [deg]
Markarian 501
3.1 - 5.5 GeV
Cumulative count
Background suppressed
Photon count
Distance from source [deg]

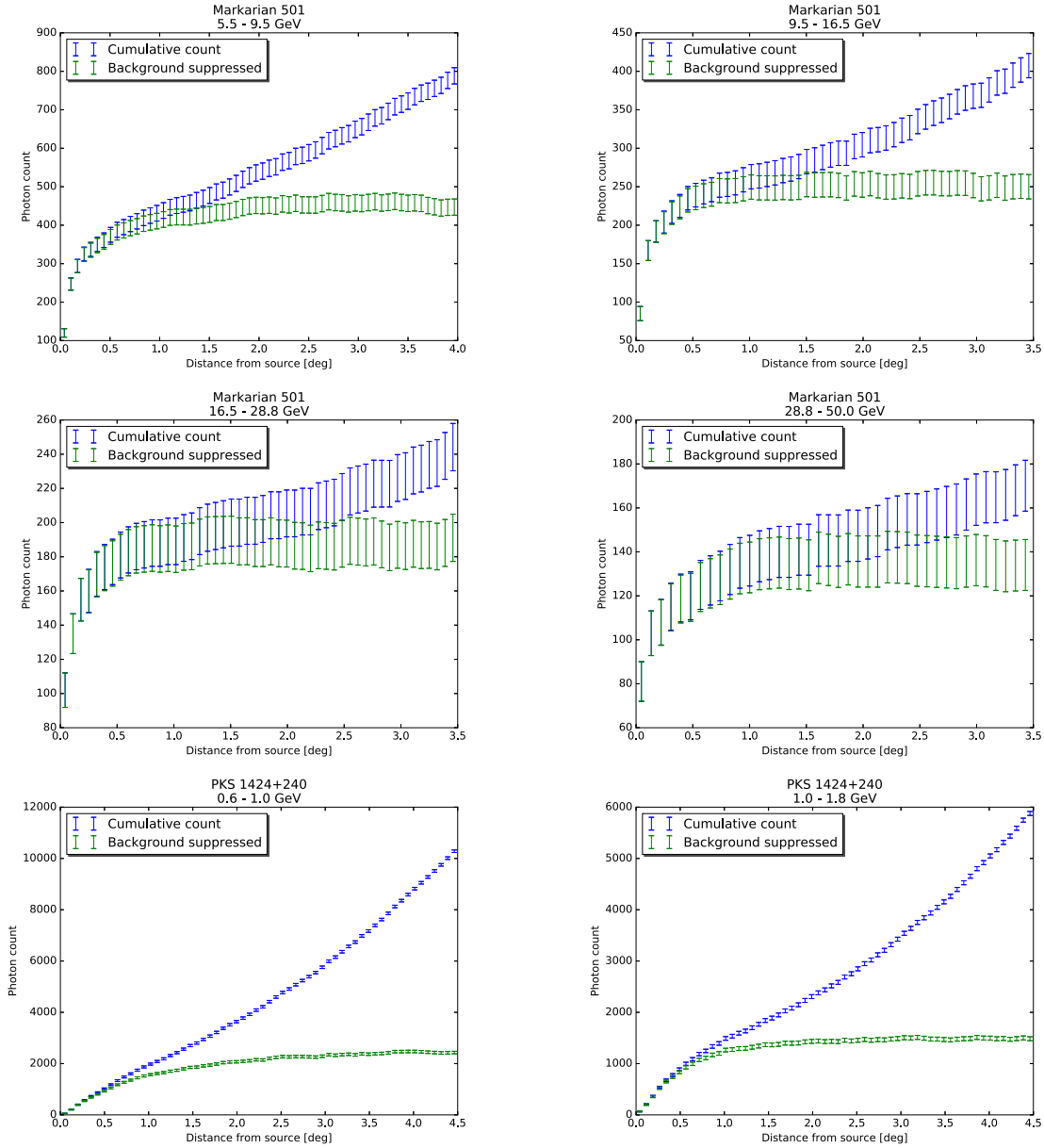
Markarian 501
5.5 - 9.5 GeV
Cumulative count
Background suppressed
Photon count
Distance from source [deg]
Markarian 501
9.5 - 16.5 GeV
Cumulative count
Background suppressed
Photon count
Distance from source [deg]
Markarian 501
16.5 - 28.8 GeV
Cumulative count
Background suppressed
Photon count
Distance from source [deg]
Markarian 501
28.8 - 50.0 GeV
Cumulative count
Background suppressed
Photon count
Distance from source [deg]
PKS 1424+240
0.6 - 1.0 GeV
Cumulative count
Background suppressed
Photon count
Distance from source [deg]
PKS 1424+240
1.0 - 1.8 GeV
Cumulative count
Background suppressed
Photon count
Distance from source [deg]

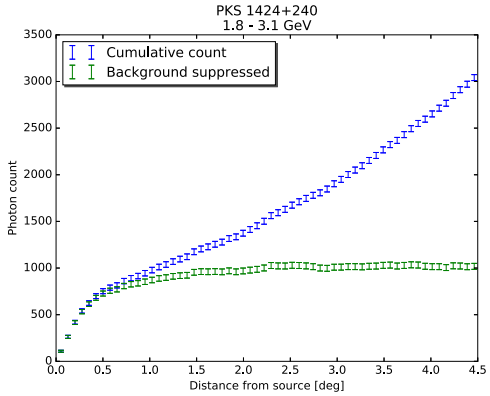
PKS 1424+240
1.8 - 3.1 GeV
Cumulative count
Background suppressed
Photon count
Distance from source [deg]

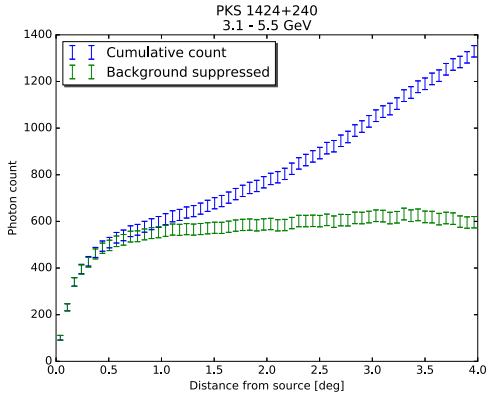
PKS 1424+240
3.1 - 5.5 GeV
Cumulative count
Background suppressed
Photon count
Distance from source [deg]

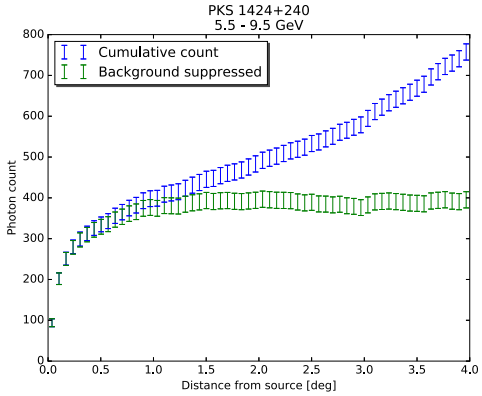
PKS 1424+240
5.5 - 9.5 GeV
Cumulative count
Background suppressed
Photon count
Distance from source [deg]

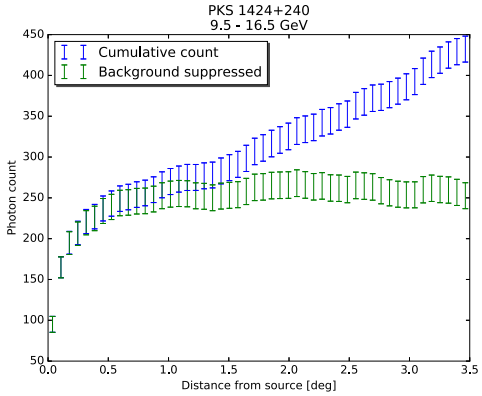
PKS 1424+240
9.5 - 16.5 GeV
Cumulative count
Background suppressed
Photon count
Distance from source [deg]

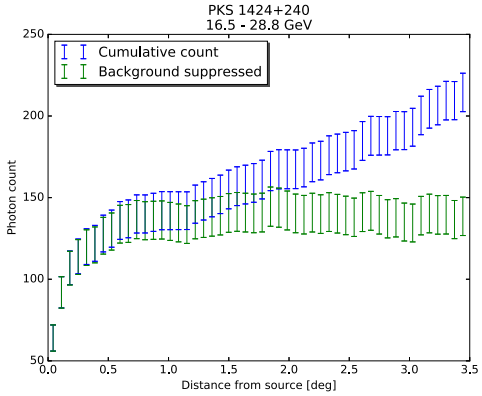
PKS 1424+240
16.5 - 28.8 GeV
Cumulative count
Background suppressed
Photon count
Distance from source [deg]

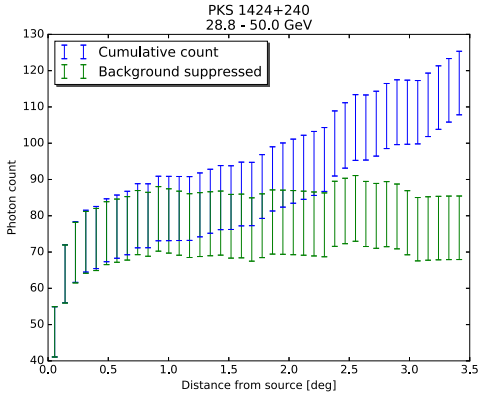
PKS 1424+240
28.8 - 50.0 GeV
Cumulative count
Background suppressed
Photon count
Distance from source [deg]

Candidate vs PSF

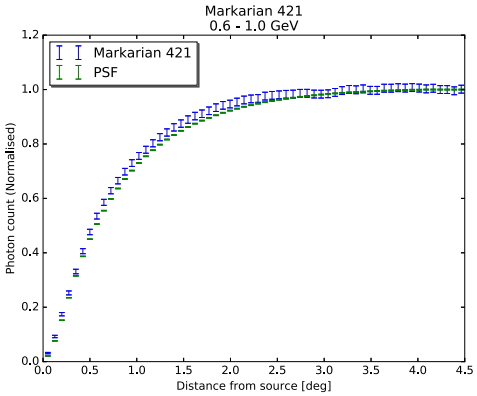

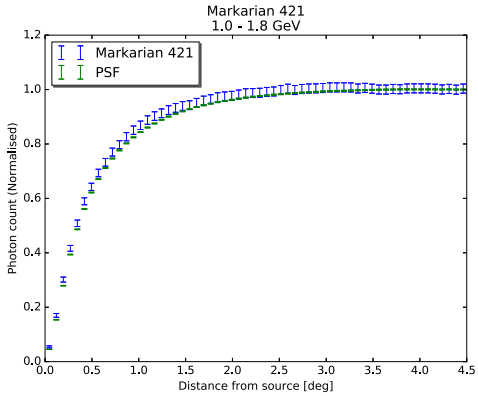

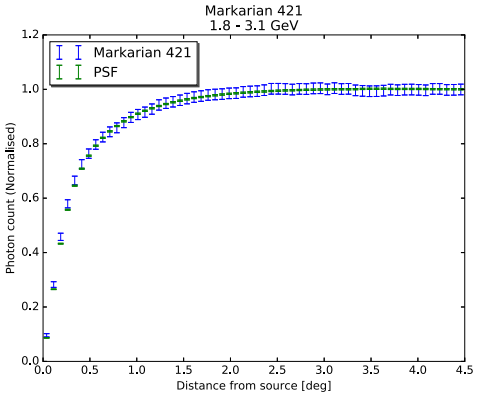

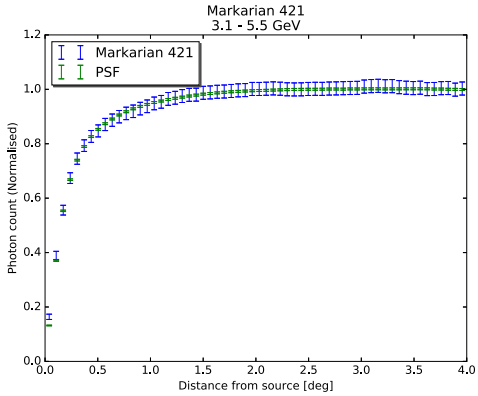

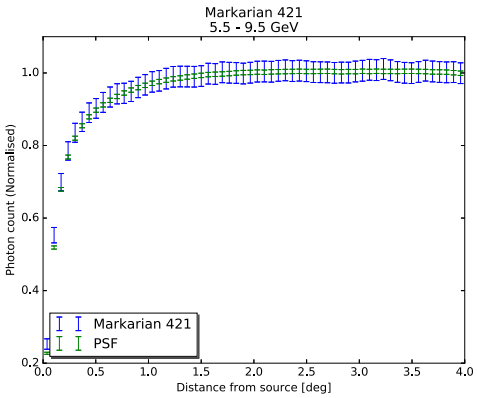

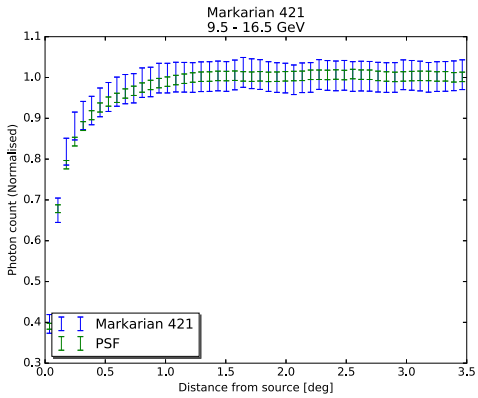

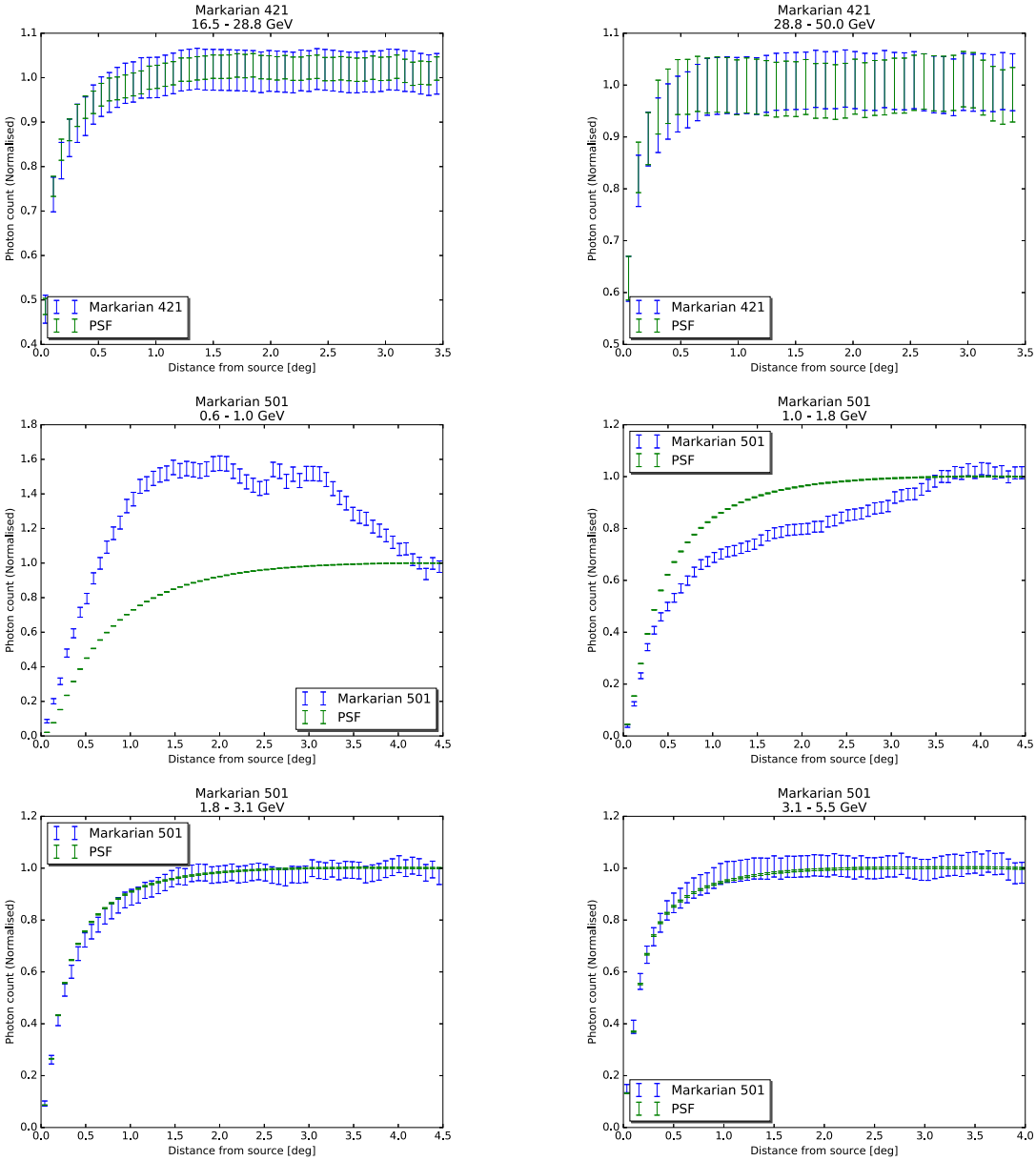
Markarian 421
16.5 - 28.8 GeV
Markarian 421
28.8 - 50.0 GeV
Markarian 501
0.6 - 1.0 GeV
Markarian 501
1.0 - 1.8 GeV
Markarian 501
1.8 - 3.1 GeV
Markarian 501
3.1 - 5.5 GeV
Markarian 421
Markarian 501
PSF
Photon count (Normalised)
Distance from source [deg]

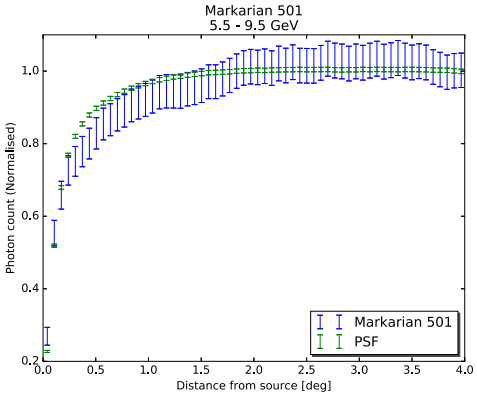
Markarian 501
5.5 - 9.5 GeV
Photon count (Normalised)
Distance from source [deg]
Markarian 501
PSF

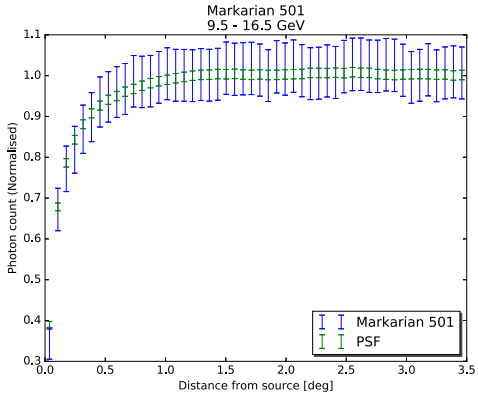
Markarian 501
9.5 - 16.5 GeV
Photon count (Normalised)
Distance from source [deg]
Markarian 501
PSF

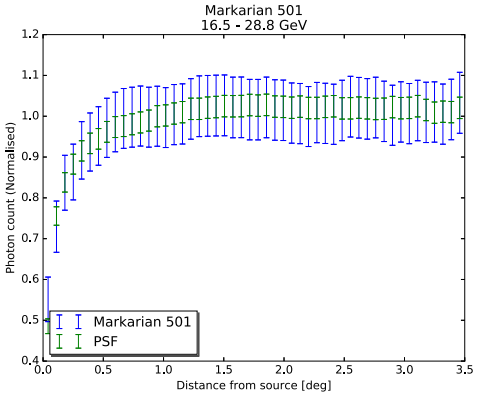
Markarian 501
16.5 - 28.8 GeV
Photon count (Normalised)
Distance from source [deg]
Markarian 501
PSF

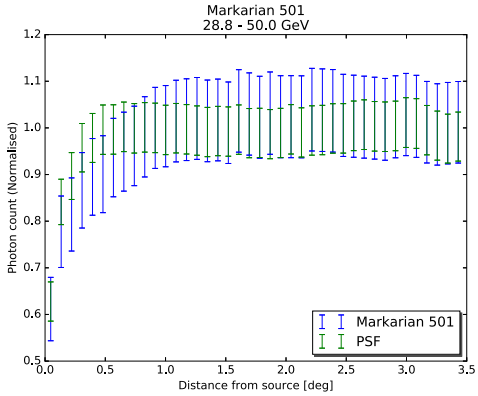
Markarian 501
28.8 - 50.0 GeV
Photon count (Normalised)
Distance from source [deg]
Markarian 501
PSF

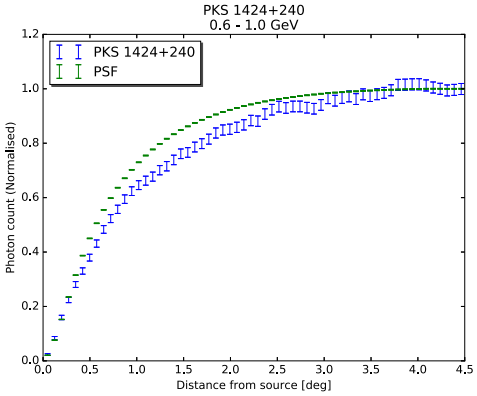
PKS 1424+240
0.6 - 1.0 GeV
Photon count (Normalised)
Distance from source [deg]
PKS 1424+240
PSF

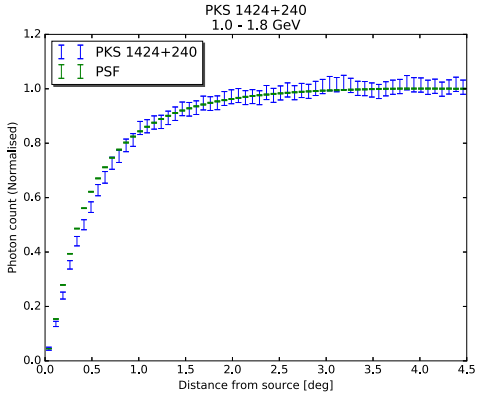
PKS 1424+240
1.0 - 1.8 GeV
Photon count (Normalised)
Distance from source [deg]
PKS 1424+240
PSF

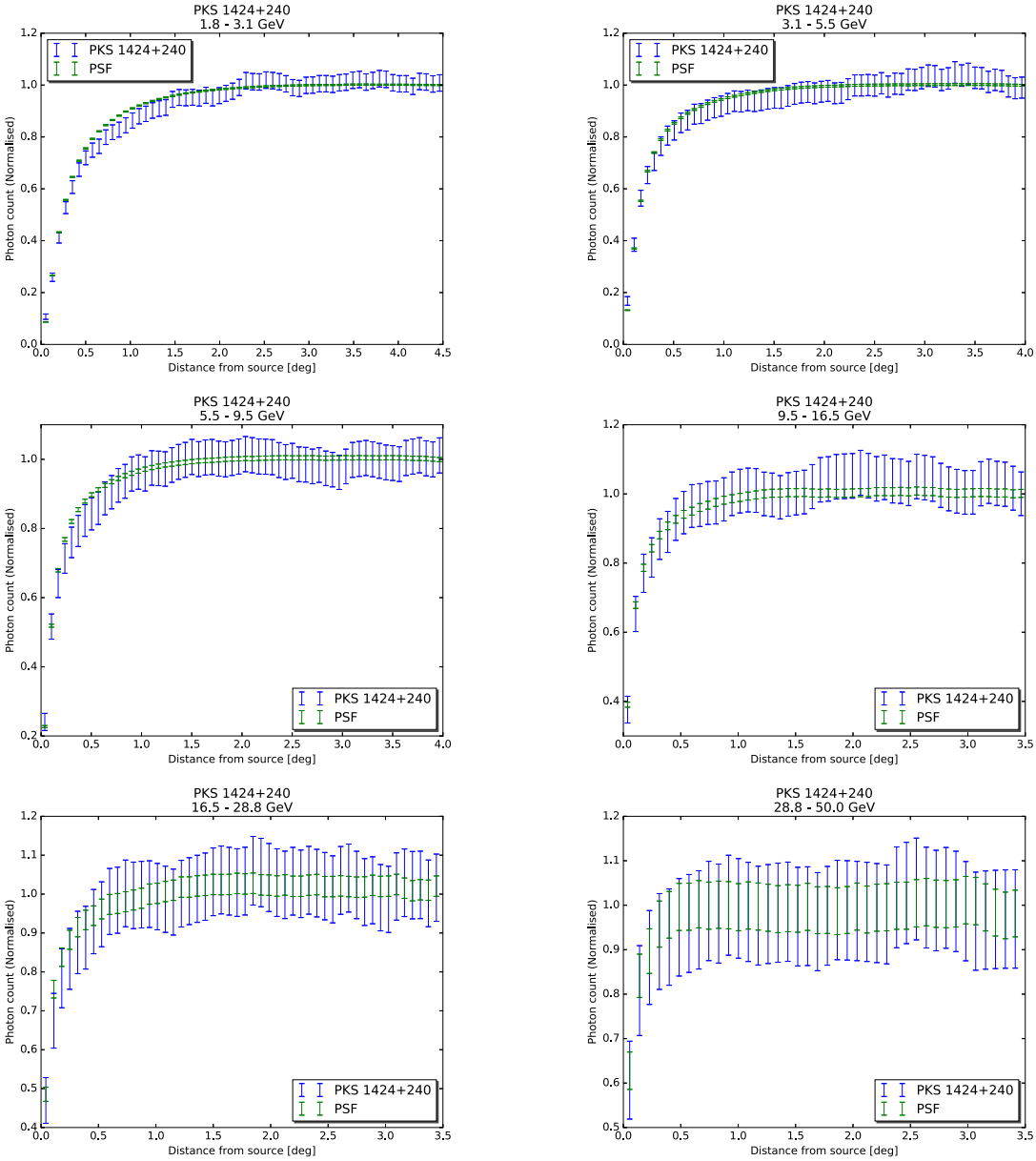
PKS 1424+240
1.8 - 3.1 GeV
PKS 1424+240
3.1 - 5.5 GeV
PKS 1424+240
5.5 - 9.5 GeV
PKS 1424+240
9.5 - 16.5 GeV
PKS 1424+240
16.5 - 28.8 GeV
PKS 1424+240
28.8 - 50.0 GeV
PKS 1424+240
PSF
Photon count (Normalised)
Distance from source [deg]